UNIVERSIDADE FEDERAL DE JUIZ DE FORA

ENGENHARIA ELÉTRICA

PROGRAMA DE PÓS-GRADUAÇÃO EM ENGENHARIA ELÉTRICA

Caique Rocha Miranda

Energy Reliability in Macro Base Stations: A Feasible Solution based on the
Singleton Type-1 Mandani Fuzzy System

Juiz de Fora

2020

Caique Rocha Miranda

Energy Reliability in Macro Base Stations: A Feasible Solution based on the Singleton Type-1 Mandani Fuzzy System

Orientador: Prof. Dr. Moisés Vidal Ribeiro

Coorientador: Prof. Dr. Fabrício Pablo Virgínio de Campos

Juiz de Fora

2020
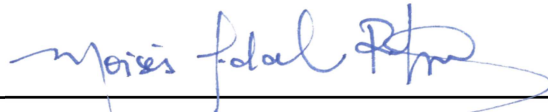
Caique Rocha Miranda

Energy Reliability in Macro Base Stations: A Feasible Solution based on the Singleton Type-1 Mandani Fuzzy System

Dissertação apresentada ao Programa de Pós-Graduação em Engenharia Elétrica da Universidade Federal de Juiz de Fora, na área de concentração em sistemas eletrônicos, como requisito parcial à obtenção do título de Mestre em Engenharia Elétrica.

Aprovada em 20 de novembro de 2020
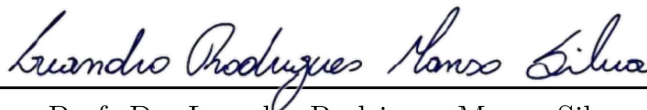
BANCA EXAMINADORA

Prof. Dr. Moisés Vidal Ribeiro - Orientador
Universidade Federal de Juiz de Fora
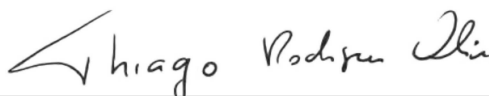
Prof. Dr. Fabrício Pablo Virgínio de Campos
Universidade Federal de Juiz de Fora

Prof. Dr. Leandro Rodrigues Manso Silva
Universidade Federal de Juiz de Fora

Prof. Dr. Guilherme Ribeiro Colen
Centro de Instrução Almirante Wandenkolk

Prof. Dr. Thiago Rodrigues Oliveira
Instituto Federal do Sudeste de Minas Gerais

ACKNOWLEDGEMENTS

"There is no progress without effort, victory without struggle, improvement without sacrifice, just as there is no tranquility without patience."

(Emmanuel).

RESUMO

As empresas de telecomunicações têm sofrido perdas financeiras devido a multas causadas por interrupções de serviço em suas Estações Rádio Base (BSs). As faltas de energia nesses locais representam um dos principais problemas da interrupção do serviço. Devido ao crescimento surpreendente no uso de redes celulares, as empresas de telecomunicações estão sendo desafiadas a melhorar consideravelmente a sua cobertura, o que significa que precisarão construir novas BSs e reformar as já existentes. Com isso, o consumo de energia aumentará significativamente e, como consequência, a avaliação da confiabilidade energética constitui uma importante ferramenta para definir em quais circunstâncias um conjunto de fontes de energia pode garantir o abastecimento de energia de uma BS. Nesse sentido, esta dissertação discute os benefícios oferecidos por uma solução viável, capaz de monitorar e gerenciar fontes renováveis ou não de energia para melhorar a confiabilidade energética das BSs *on-grid* e *off-grid*. Na sequência, a dissertação aborda como a solução viável em uma BS macro pode operar quando concessionária de energia, geração eólica, geração solar, gerador a diesel e banco de baterias estão disponíveis. Nesse sentido, surge a utilização do Sistema Fuzzy Mamdani Tipo-1 (T1FS) com o defuzzificador centróide, que se propõe a realizar de forma dinâmica a escolha da fonte de energia que irá alimentar a BS macro. Para alcançar uma carga computacional baixa, o T1FS com o defuzzificador por altura também é sugerido. A utilização do defuzzificador por altura exige a adoção de um método de treinamento para obtenção de seus parâmetros e, como consequência, o uso do método *steepest descent* é brevemente discutido. Além disso, sugere-se a adoção da função de confiabilidade para fornecer um modelo probabilístico capaz de quantificar a confiabilidade da energia em uma BS macro quando um determinado conjunto de fontes de energia está disponível. Ademais, sinaliza-se que a teoria da confiabilidade pode ser uma ferramenta adequada para auxiliar as empresas de telecomunicações a prever a confiabilidade energética em uma BS em diferentes cenários e, por consequência, mitigar ou eliminar as perdas associadas à falta de confiabilidade energética em uma BS.

Palavras-chave: Estação rádio base. Energias renováveis. Energias não renováveis. Função de confiabilidade. Sistema fuzzy.

ABSTRACT

Telecommunication companies have suffered financial losses due to penalties caused by service interruptions in their Base Stations (BSs). The power outages in these places represent one of the main problems of the service interruption. Due to the surprising growth in the use of cellular networks, telecommunications companies are being challenged to remarkably improve their coverage, which means that they will need to build new BSs and retrofit the existing ones. In this sense, energy consumption will significantly increase and, as a consequence, the evaluation of energy reliability constitutes an important tool for defining in which circumstances a set of energy sources can ensure the supply of a BS. In this regard, this thesis discusses the benefits offered by a feasible solution that is capable of monitoring and managing renewable or not sources of energy for improving energy reliability in BSs (on- and off-grid). In the sequel, it addresses how the feasible solution in a macro BS can operate when power utility, wind generation, solar generation, diesel generator, and battery bank are available. In this sense, the use of the Mamdani Type-1 Fuzzy System (T1FS) with the centroid defuzzifier, which is proposed to dynamically perform the choice of an energy source that will feed the macro BS. For achieving a low computational burden, the Mamdani T1FS with the height defuzzifier is also suggested. The use of the height defuzzifier demands the use of a training method for obtaining its parameters and, as a consequence, the use of the steepest descent method is briefly outlined. Furthermore, it is suggested the adoption of the reliability function for providing a probabilistic model that is capable of quantifying the energy reliability in a macro BS when a certain set of energy sources is available. Also, it points out that the reliability theory can be an appropriate tool to assist telecommunication companies to predict energy reliability in a BS in different scenarios and, as a consequence, to mitigate or eliminate the losses associated with the lack of energy reliability in a BS.

Keywords: Base station, renewable energy, non-renewable energy, reliability function, fuzzy system.

LIST OF FIGURES

LIST OF TABLES

ACRONYMS

CONTENTS

1 INTRODUCTION

The current decade is facing an astonishing growth in the telecommunication sector. In fact, the necessity of connectivity among users and things are pushing forward the telecommunication industry to advance new standards and introduce pervasive, diverse, and flexible telecommunication infrastructures and technologies. It is well-known that the number of users and the demand for cellular traffic have been dramatically increased because of the growing dependency of human beings on smart things technologies, such as smartphones and devices for deploying the Internet of Things (IoT), smart city, Smart Grid (SG), and Industry 4.0 solutions [1]-[9]. In this sense, widespread and expressive Research and Development (R&D) efforts to come up with Fifth Generation (5G) and Sixth Generation (6G) cellular technologies have been carried out by the main stakeholders in the telecommunication sector. In fact, as well predicted in the technical literature [10], the massive deployments of anywhere, anytime and anything technologies are demanding an exponential increase of the data traffic. As a result, telecommunications companies inevitably are seeking to meet these demands updating and improving cellular networks.

In addition to the current growth of the telecommunications market and its increasing prediction in the next decades, the year of 2020 will be marked the year of coronavirus pandemic (COVID-19) [11], in which many companies, due to the lockdown, are adopting the home office for their employees, the e-commerce segment is facing a remarkable growth, business meetings are being heavily based on videoconferencing, the Live concerts streaming is showing a significant increase, remote teaching is becoming massive, and the massive processing of online legal routines [12]. As a consequence, explosive demands for pervasive and flexible telecommunications infrastructures are occurring in 2020 [13]. According to the Brazilian Telecommunication Regulatory Authority, the telecommunications service providers have been expanded their telecommunication infrastructures to deal with these remarkable traffic demands [14]. Moreover, after the end of the coronavirus pandemic, it is predicted that many companies are going to adopt the home office, once it can offer several advantages for them and their employees. Also, new habits heavily relying on pervasive and flexible telecommunication infrastructures will become normal in our society.

A key piece of technology for assisting the telecommunication companies to fulfill the users' demands related to cellular traffic is the so-called Base Stations (BSs), which is going to be massively used in 5G and 6G cellular technologies. However, a large number of BSs means that energy consumption and reliability start to play a pivotal role because they constitute a *sine qua non* condition to ensure that BSs will effectively operate on 24 hours-a-day and 7 days-in-a-week. It is well-known that the energy consumption per bit is steadily reducing, but the throughput is increasing at a faster rate. In this sense, energy reliability in a BS must be correctly addressed. In this scenario, in addition to the electricity provided by a power utility, the use of renewable energies (e.g., solar and

wind) and/or non-renewable (e.g., diesel generator) will be relevant to feed BSs in several conditions [15]. Note that BSs can be on-grid or off-grid[1] mainly in urban and rural areas, respectively.

Considering energy reliability in BSs, it is of fundamental importance to model their power consumption. In this sense, [16] described a sophisticated power model for various BSs types that allows relating the Radio Frequency (RF) output power radiated by the antennas to the total power necessary to operate a BS while [17] analyzed the power consumption of small BSs for 5G technologies, which adopt massive Multiple-Input Multiple-Output (MIMO) and millimeter-wave technologies. In addition, [18] proposed a power consumption model for both macro and micro BSs[2] and validated it by using power consumption measurements taken from several BSs. According to [18], a macro BS consumes about 4.4x more power than a micro BS; however, a micro BS is less energy-efficient than a macro BS from a telecommunication perspective, because it covers a smaller spatial range. Moreover, [19] developed linear power consumption models based on real on-site measurements obtained from a set of macro BSs deployed between 2000 and 2012 and they are capable of modeling the current generations of cellular technologies. These models are developed by means of linear regression and take into account the influence of transmit power on the instantaneous power consumption of macro BSs for Second Generation (2G), Third Generation (3G), and Fourth Generation (4G) technologies.

Regarding the use of different energy sources in BSs, [20] briefly discussed the green (renewable) power generation together with BS power consumption models. Also, it investigated how to design and optimize green energy powered BSs by provisioning the green power system and optimizing the management of the available energy resource in BSs. [21] proposed a model for the cooperation between two cellular BSs, which make use of power utility and renewable energy sources, with the purpose of minimizing the total energy consumption. [22] discussed how a BS can control the use of renewable energy sources and power utility based on the Nash equilibrium concept. Simulation results have shown that using green energy powered BS yields a significant electric energy saving. [23] presented a review of different energy source solutions for feeding off-grid BSs and discussed key aspects in choosing and designing appropriate energy source solutions for feeding BSs. These solutions may include distinct energy sources (e.g., diesel generator, solar generation, or wind generation) and different combination of energy sources (i.e., solar-wind generation, solar-diesel generation, solar-wind-diesel generation, and solar-fuel cell generation) together with a specific energy storage capacity (e.g., battery bank, hydrogen, and the combination battery-hydrogen). [24] discussed and, as a consequence, classified the existing renewable

---

[1]   On-grid and off-grid mean that BSs are connected or not to the power utility, respectively.

[2]   BSs are divided into macro cells and small cells, named as macro or small BSs, which the former presents larger spatial coverage and power consumption when compared to the latter. In descending order of spatial coverage and the power consumption, the small BSs integrates femto BSs, pico BSs, micro BSs, and distributed Remote Radio Head (RRH) technologies [16].

energy-powered BSs solutions and proposed a new architecture for integrating renewable energy-powered BSs together with SG. [25] examined the feasibility and effectiveness of the integration of a solar generation with the biomass source generation for feeding off-grid macro BSs in Bangladesh and, as a consequence, minimizing the life-cycle cost and greenhouse gas emissions. They showed considerable savings can be attained by using such kind of solutions. [26] proposed an energy-aware management system that aims to limit the amount of purchased energy from power utility using a realistic small-scale Long Term Evolution (LTE) cellular network fed by solar generation and power utility. In this sense, the authors showed that an energy-aware strategy is very useful since it can reduce the energy consumption between 21% and 41% when solar generation is wisely consumed.

A comprehensive overview of resource management in BSs powered by renewable energy sources and deep analysis of power consumption was addressed in [27]. In addition, [28] studied powering systems for LTE macro BSs that make use of solar generation or a mix of solar generation and power utility. They formulated the problem of the optimal choice of the solar panel size and number of batteries with a Mixed Integer Programming problem. The results showed that hybrid energy generation systems (solar and power utility) are more effective than a pure solar one. [29] evaluated costs and CO^2 emissions savings in the scenario addressing only power utility in all BSs and in the scenario based on the use of solar generation in micro and small BSs and power utility in macro BS. [30] used an adaptive energy management system for feeding BS through the SG when renewable energy sources are used. It showed that renewable energy sources are firm alternatives for reducing the energy cost and the CO_2 emission and concluded that an adaptive power management system can successfully accomplish these aims. Also, [31] analyzed economics issues, and greenhouse gas emission in on-grid BS considering power utility, solar generation, and wind generation while [32] dealt with the use of renewable energy sources at a BS operating as a relay nodes for reducing the overall cost of consumed energy. [33] focused on two different energy management schemes for heterogeneous cellular networks powered by hybrid energy sources. In the former, a reactive user equipment-BS association scheme operating over the short-time scale aims to prioritize renewable energy consumption over power utility one by choosing BS nodes powered by renewable energy. In the latter, predictive actions are taken for minimizing the energy delivery by power utilities in a long-time scale based on the adoption of traffic flow planning. The authors showed that the use of energy management tools decreases in energy consumption by the power utility and, as a consequence, the cost with energy. [34] investigated the problem of energy cost reduction in a BSs when hybrid energy sources are combined with a sleep mode technique. They authors showed that a Lyapunov-based technique can achieve approximately minimal energy cost for BS. [35] studied cellular networks fed by solar generation and power utility in IoT environment, and proposed a BS sleeping algorithm based on coalitional games for ensuring communication service quality and power utility

energy-saving. The authors showed that the proposed algorithm performs excellently in improving solar generation utilization and reducing the energy consumption of the power utility. In addition, [36] studied how to reduce the total energy cost in a green heterogeneous cellular network with hybrid energy sources. They formulated a total cost minimization problem and decomposed it into four sub-problems that resulted in the Energy Consumption Estimation (ECE) algorithm, the Green Energy Allocation (GEA) algorithm, the User Association (UA) algorithm, and the Green Energy Reallocation (GER) algorithm. Simulation results showed the effectiveness of the proposed algorithm to come up with energy cost reductions. [37] addressed an energy management technique for enhancing energy efficiency of an off-grid LTE macro BS by focusing on the maximum usage of renewable energy sources, which are less expensive than the electricity delivered by utilities.

The aforementioned contributions and references therein have discussed and introduced different methods and strategies to feed different types of BSs, to increase the energy efficiency of BSs connected to the power utility (on-grid) or isolated (off-grid), to decrease the energy consumption from the power utility because it is the most expensive energy source and may not be available everywhere. However, it is clear a lack of discussion about the difficulties faced by telecommunication companies regarding the unavailable services in BSs. Indeed, according to [38] the power outages represent one of the main causes of unavailable services in BSs and, as a consequence, a relevant source of fines applied to telecommunication companies. Moreover, paying attention to macro BSs, it is important to emphasize that many of them will be retrofitted to accommodate the newest generations of cellular technologies. In this regard, the use of different energy sources for decreasing power outages and, as a consequence, increasing energy reliability is an important issue to be addressed in the retrofitting process of macro BSs. In this sense, the complete potential knowledge of the energy sources for feeding macro BSs and the design of a simple and effective solution to switch among these energy sources need to be addressed for postponing the usability of these macro BSs, in which the necessity of using renewable sources is part of the worldwide green initiatives to reduce environmental pollution and global warming.

In this regard, there is a necessity of introducing feasible techniques that are capable of managing and controlling different energy sources and easy to develop and update. Indeed, these techniques will be applied to retrofit BSs and, as a consequence, they have to be simple, effective, and capable of dealing with the constraints imposed by BSs that are already in the field. Also, it is important to come up with the use of tools that are capable of evaluating the effectiveness of the combined use of energy sources in BSs in terms of energy reliability.

1.1 OBJECTIVES

Aiming to offer directions to address the aforementioned problems, the objectives of this thesis are as follows:

- To discuss the problems suffered by telecommunication companies due to the unavailability of their communication services caused by the power outages in BSs. In this regard, to describe a feasible solution for designing new BSs or retrofitting the existing ones aiming to assist the telecommunication companies to deal with those problems. The feasible solution is constituted by cloud platform and specific general-purpose hardware prototypes. The feasible solution is used for remote monitoring and managing of the available energy sources in BSs, which can operate on- or off-grid.

- To investigate the usefulness of the Mamdani Type-1 Fuzzy System (T1FS) and its design for performing the dynamic switching of the available energy sources in a macro BS. In this regard, to introduce the reliability function for allowing a statistical quantification of the energy reliability in a macro BS given a set of energy sources using a fuzzy system-based controller. It can help the telecommunication companies to predict several scenarios assisting with the decision-making process by telecommunication companies with respect to the use of different configurations of set of energy sources in a macro BS. In addition, to provide numerical analyses based on the use of a battery bank together with the combinations of energy delivered by the power utility, the wind generation, the solar generation, and the diesel generator in a macro BS. The analyses of wind and solar generations refers to real data collected in the city of Juiz de Fora, Brazil.

1.2 THESIS ORGANIZATION

The remainder of this thesis is organized as follows:

- Chapter 2 discusses the problems suffered by telecommunication companies due to the unavailability of their communication services caused by power outages and the consequences that they generate for them. In the sequel, it presents a feasible solution for improving energy reliability in BSs. Also, this chapter details the development of the main components of this feasible solution for improving energy reliability in a macro BS.

- Chapter 3 discusses a fuzzy system-based control technique that is applied for switching the available energy sources in a macro BS. In this sense, it outlines the Mamdani T1FS and two kinds of defuzzifications. The first defuzzification is based

on the centroid defuzzifier, which is more difficult to develop and demands a high computational burden. The second one is based on the height defuzzifier, which is easy to develop and presents reduced computational complexity. Also, a supervised training procedure, which is based on the steepest descent method, for dealing with the height defuzzifier is presented.

- Chapter 4 starts with the discussion about energy consumption (i.e., a power model) for a macro BS. In the sequel, it presents details of the power utility, diesel generator, solar generation, wind generation, and a battery bank for energy backup. Details about real data sets used to model solar and wind generations are provided. Also, it discusses the use of the reliability function to quantify the energy reliability in a macro BS.

- Chapter 5 discusses the boundaries for performing numerical simulations. In the sequel, it shows the designed rule base (complete and incomplete) of the Mamdani T1FS that is based on the centroid defuzzifier. Also, numerical analyses related to the dynamic use of this fuzzy system-based controller and the effectiveness of reliability function to quantify energy reliability in BSs. In the following, numerical results related to the Mamdani T1FS based on the height defuzzifier are detailed. Special attention is toward the gains that the training procedure can offer to improve the performance of this fuzzy system-based controller in comparison to the one based on the centroid defuzzifier.

- Chapter 6 summarizes the main contributions and findings related to this thesis. Also, it outlines future research endeavors and new problems that brought the attention.

1.3 SUMMARY

This chapter presented a brief introduction of this thesis, addressing energy consumption and reliability issues in BSs due to the increase in demanded numbers of BS by 5G and 6G technologies, the astonishing necessity of communications among users and things (e.g., increasing cellular traffic). Also, it summarized the technical literature about power models and the power consumption in different types of BSs. Moreover, it discussed different methods for feeding different types of BSs and strategies to increase the energy efficiency of on-grid or off-grid BSs, presenting a lack of discussion about energy reliability. Finally, the main objectives and the organization of this thesis were detailed.

2 RETROFITTING MACRO BASE STATIONS: A FEASIBLE SOLUTION

The necessity of providing connectivity among users and things has been pushing forward the telecommunications industry to advance new standards and technologies for introducing pervasive and flexible telecommunications infrastructures. Indeed, the demands for cellular traffic have increased dramatically due to the growing dependence of human beings on telecommunication technologies, such as mobile. In this sense, there has been a continuous development of mobile networks, with 4G being the most used technology today, to deal with the telecommunication demands forecasts. In addition, significant investments in 5G and 6G cellular technologies have been made by the main stakeholders in the telecommunications sector [39]. As a result, telecommunications companies are inevitably looking for meeting these demands by updating and improving cellular networks. In this regard, the BSs play an important role to ensure that cellular networks work properly (e.g., Quality of Service (QoS) guarantee, reliability, and coverage). In this sense, the occurrences of power outages at a BS must, by all means, overcame because it negatively impact the provision of the telecommunication service and, as a consequence, the telecommunication companies may be penalized with fines because of the lack of reliability.

In this regard, this chapter details the problem suffered by telecommunication companies due to the unavailability of their communication services caused by power outages. Paying attention to BSs, it discusses the development of a feasible solution, for dealing with renewable and non-renewable energy sources, that can be added to improve the energy reliability in the existing macro BSs in the field. It is important to mention that the focus is on macro BS because it allows us to define the boundaries of the energy reliability problem and, as a consequence, to come up with numerical simulations that can be used for evaluation purposes. However, it is important to emphasize that the whole solution can be easily adapted to fit other kinds of BSs in the field or be introduced in the new ones. Also, this chapter discusses the development of the main components of the feasible solution by detailing the cloud platform, prototyped hardwares, and technologies on the shelf. The use of the chosen on the shelf technologies fulfills the specification for dealing with the posed problem and speed up the development process.

In this context, this chapter is organized as follows: Section 2.1 formulates the investigated problem. In the sequel, Section 2.2 discusses the feasible solution for BS. Section 2.3 outlines the development of the feasible solution in a single macro BS. Finally, Section 2.4 addresses a brief summary of this chapter.

2.1 PROBLEM STATEMENT

A BS consists of a set of equipment (e.g., antenna, power amplifier, processors, battery, etc) installed at a telecommunication facility [40].A BS is a radio receiver/transmitter that works as a hub of a local wireless network or may be a gateway between a wired network and a wireless network. Due to the distinct generations of wireless network technologies, the BSs are divided into macro cells and small cells, named as macro or small BSs. The small BSs integrates femto BSs, pico BSs, micro BSs, and distributed RRH technologies [16]. The spatial coverage and the power consumption of macro BSs are higher in comparison to a small BSs [41]. A macro BS is a cell in a telecommunication network that provides radio coverage served by a high power BS. The femto BSs, pico BSs, micro BSs, and distributed RRH technologies consume around 0.6%, 0.9%, 9.7%, and 54.7% of the energy consumed by a macro BS, respectively [16]. Note that the transmission power determines the spatial coverage of a BS. In addition, the transmission power influences the traffic capacity of the wireless network, which is proportional to the cell size. It is important to emphasize that macro BSs exert relevant importance in the spatial coverage of wireless networks, mainly to provide mobile access in urban areas. Giving the necessity of guaranteeing 24/7 (i.e., 24 hours a day, 7 days a week), telecommunications companies are compelled to ensure energy reliability in macro BSs because the lack of it is one of the main sources of telecommunication services unavailability.

Regarding reliable telecommunication services, telecommunications companies may suffer remarkable economic losses with fines due to their telecommunication service interruptions. It has been recognized that power outages at BSs facilities are one of the main sources of service interruptions. Interruptions resulted in financial sanctions about R$ 740 million in 2016 in Brazil [38]. According to the Brazilian Telecommunication Regulatory Authority, Table 1 summarizes the underlying causes of service interruptions of Multimedia Communication Service (MCS), Personal Mobile Service (PMS), and Switched Fixed Telephony Service (SFTS) at BSs in Brazil [38]. The values in this table show that power outages define a substantial problem to deal with. Note that power outages may become a worse issue if BSs are located in isolated and difficult to access places. In this case, it takes more time for recovering BSs from the ongoing power outages if a crew is necessary to perform local maintenance. In other words, the recovery of a BS in these places is more time consuming and, as a consequence, more expensive when compared to BSs located close to the telecommunication companies.

On August 4th, 2018, the Brazilian Telecommunication Regulatory Authority finalized the Public Consultation 29/2017 [42], which carried out to collect subsidies on the proposed revision of the norms and the procedures for monitoring and controlling the quality of services. As established in the quality management regulations for fixed broadband and mobile telephony, described by Resolutions 574/2011 and 575/2011 [43] [44],

and updated by Resolution 717/2019 [45], the Brazilian Telecommunication Regulatory Authority monitors the indicators that demonstrate the performance of the networks in relation to parameters such as speed, connection rate, latency, packet loss, and availability. Availability is defined as the percentage of effective time in which the entire network in a given geographical area was fully available to the complete enjoyment of the service [43]. In this way, the power outage impacts the calculation of the availability parameter defined by the Brazilian Telecommunication Regulatory Authority in relation to the time of the fault and in relation to the affected area.

The fault time is directly linked to the repair time in a possible BS and this time can be aggravated since the location of the BSs are generally difficult to access and away from the telecommunication control centers. In this way, it is essential to assess solutions capable of minimizing downtime by means of signaling and the possibility of remote management. In this way, this thesis use the energy reliability parameter as a metric for evaluating the availability of the services provided, aiming at the greatest availability, thus the greatest energy reliability.

Table 1 – Statistics of interruption in telecommunications services in Brazil in percentage (%).

Use	Interruption	2013	2014	2015	2016
MCS	Power outage	9.1	21.3	23.5	23.2
	Vandalism	14.9	9.0	5.0	3.7
	Others	75.9	69.7	71.5	73.0
	Total	100.0	100.0	100.0	100.0
PMS	Power outage	37.7	19.0	18.4	13.5
	Vandalism	1.3	1.9	2.3	2.0
	Others	61.0	79.1	79.2	84.6
	Total	100.0	100.0	100.0	100.0
SFTS	Power outage	12.6	10.8	9.5	8.0
	Vandalism	4.1	5.1	4.4	5.0
	Others	83.3	84.1	86.2	87.0
	Total	100.0	100.0	100.0	100.0

Regarding power outages in BSs, there is a research opportunity to deal with the intermittent availability of electricity provoked by the use of only one energy source to feed BSs. In this sense, it is important to investigate how to perform the combination of distinct energy sources for ensuring energy reliability in BSs. These energy sources can be renewable (for example, wind and solar ones) and non-renewable (for example, diesel generator) that are combined to the power utility. The investigation of the combination of different sources of energy for feeding BSs may allow telecommunications companies to postpone or eliminate power outages in BSs and, as a consequence, to reduce economic losses due to revenue reduction and penalties related to the breach of contracts. Also,

this kind of investigation can result in a methodology and simulator that can analyze the energy reliability based on the system reliability theory to help the telecommunication companies to predict when power outages may occur in BSs and, as consequence, to assist the telecommunication companies to reduce the fines with unavailability services.

Aiming to offer directions to address the aforementioned problem, this chapter discusses a feasible solution for ensuring energy reliability in existing BSs (i.e., retrofitting) or new ones. Due to its simplicity and the use of technologies on the shelf, it can be easily adapted to operate in any size of BSs and cover functionalities that address other demands, such as security. This feasible solution consists of a cloud platform and specific general-purpose hardware prototypes. The feasible solution is used for remote monitoring and management of the energy sources available in the BSs, which can operate on- or off-grid, and to smartly control the switching among the sources of energy that are available for feeding a macro BSs.

In this regard, Section 2.2 discusses how telecommunication companies can manage their energy sources and decrease power outages using a detailed feasible solution for BSs and, consequently, increase the energy reliability in those places.

2.2   A DISCUSSION ABOUT A FEASIBLE SOLUTION FOR BASE STATIONS

There is a trend in the use of IoT concepts (i.e., monitoring and remote control) due to the low cost that these solutions can offer [1]. In this regard, using the concepts of IoT could offer a very simple solution for designing new BSs or retrofitting the existing ones. With the use of a solution based on these concepts, several sensors could be added to the energy sources of the BSs to monitor the behavior over time of the generation of electrical energy. Based on the data generated by the reading of these sensors, could be created a smart controller to carry out the control of energy sources automatically in each BS itself.

In this regard, this section discusses a feasible solution to investigate the design of new BSs or retrofit the existing ones, aiming to assist telecommunications companies to deal with the problems of the unavailability of services caused by power outages. This feasible solution consists of a cloud platform and general-purpose hardware prototypes. The feasible solution is used for remote monitoring, management, and controlling of the energy sources available in the BSs, which can operate on- or off-grid.

Figure 1 shows the proposed feasible solution for BSs (on- and off-grid) that focuses on monitoring and controlling renewable and non-renewable energy sources in order to provide uninterrupted energy delivery for BSs. This feasible solution can be applied to on-grid and off-grid BSs. In this sense, with this feasible solution for BSs it is possible to study possible scenarios using different set of energy sources for feeding BSs. Also, to create a methodology to study of energy reliability and assist telecommunication
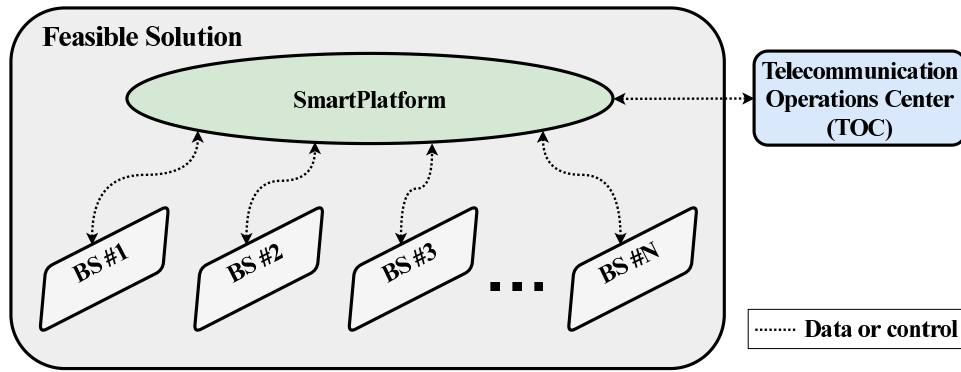
Figure 1 – A feasible solution for BSs.

companies concerning the use of different energy sources for feeding BSs. In addition, it is possible that the telecommunications companies evaluate and predict possible events of unavailability of the service and, thus, minimize the economic losses caused by these events. Also, telecommunications companies can predict when the power outages would occur in their BSs. Moreover, this study is interesting to predict the time that telecommunications companies would have to repair their energy sources with fails considering scenarios where other energy sources are feeding the BSs. This feasible solution is constituted of three parts that are described as follows:

- **BS #n**: the feasible solution for n-th BS covers the sensors, which are responsible for acquiring data related to physical quantities (e.g., temperature, current, voltage, wind speed, solar radiation, diesel tank level, battery charging, etc) related to energy sources. Also, equipment composed of hardware and firmware that are used in the feasible solution for the n-th BS for receiving and processing the information collected by the sensors. In addition, the data collected by sensors related to the energy sources can be used as input parameters in a smart controller, which based on this data could select dynamically the energy source to feed the BS #n. The BS #n communications with the Telecommunication Operations Center (TOC) through the SmartPlatform. Index #n refers to the n-th BS and N is the total number of BS (i.e., $1 \leqslant n \leqslant N$).

- **SmartPlatform**: it is the platform responsible for exchanging all types of data between the BSs and a TOC. Also, it is responsible for monitoring, updating, and controlling all BSs. This platform is constituted by two components: ServerPlatform and WebPlatform. The former saves the received data by BSs in a database, while the latter owns a friendly-user interface and connects to the former to access the information of the database. The ServerPlatform and WebPlatform run in the server at the TOC.

- **Telecommunication Operations Center**: it is the center of control and monito-

ring where telecommunications company monitor in real-time the operation of the BSs. The connection among TOC and BSs makes use of a computer that connects to an WebPlatform in the SmartPlatform. After connecting, telecommunication companies can remotely manage all BSs, receiving data and sending commands. Also, the use of alarm scheduling based on predictions of scenarios is also possible.

The feasible solution for BSs defines two types of data communication technologies. One of them is applied to connect all devices inside the BS. The other refers to the communications among all BS to SmartPlatform. A brief description of these types of technologies is as follows:

- **Data exchanges among devices inside a BS**: the area in which the BSs are installed are taken into account. The equipment related to the energy sources can be installed inside or outside of the building of the BSs. As a result, wireline or wireless technology may be used. An advantage related to the use of a wireline technology refers to the fact that shielded cables can offer the quality of service to assist energy reliability.

- **Data exchanges among BSs and SmartPlatform**: it can be accomplished by using an available or dedicated link in the BS. In general, a BSs located in rural areas will demand wireless technologies, while the others located in urban areas will make use of wireline or wireless technologies.

Based on the information presented in this section, Section 2.3 shows the development of a feasible solution applied in a macro BS.

2.3 A DEVELOPMENT OF THE FEASIBLE SOLUTION IN A MACRO BASE STATION

There is a large number of macro BSs and they need to be retrofitted or upgraded for supporting the establishment of reliable telecommunication infrastructures. In this regard, Figure 2 shows the block diagram to represent the development of the feasible solution for improving the energy reliability in a macro BS when power utility, solar generation, wind generation, diesel generator, and battery bank are used to improve the energy reliability. Note that solar generation and wind generation work together with the battery bank because they are, by nature, intermittent sources of energy. The energy is stored in the battery bank for controlled use by macro BS. Also, the Alternating Current (AC) voltages used at the power utility and diesel generator are rectified to Direct Current (DC) voltage by rectifier device. This is necessary to adapt the energy to the electrical characteristics necessary for equipment inside the macro BS. Additional information about the energy sources, battery bank, and macro BS power are in Chapter 4.
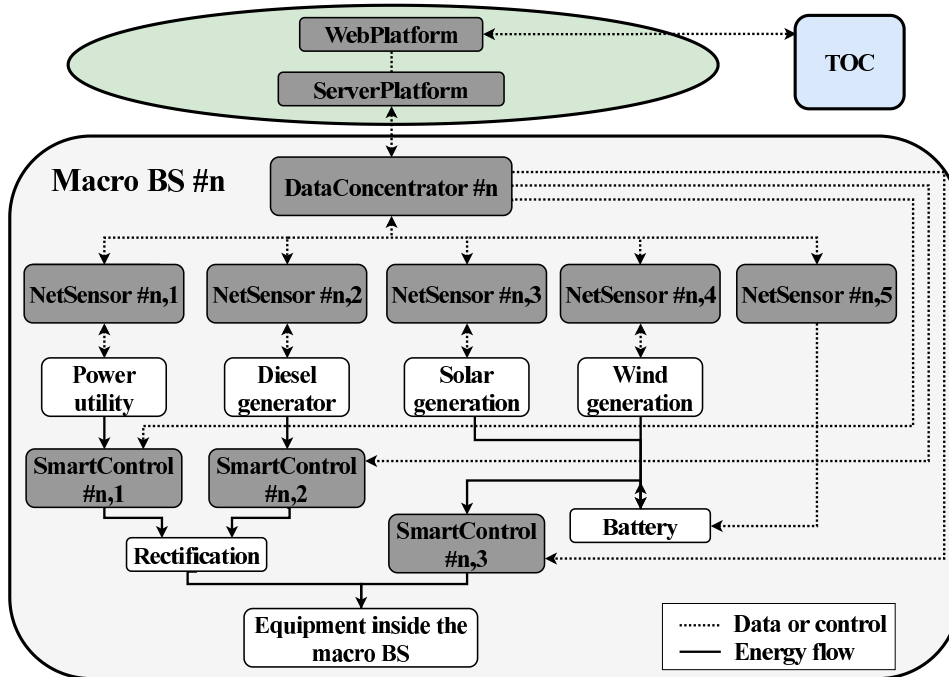
Figure 2 – The development of the feasible solution in a macro BS.

According to Figure 2, the SmartPlatform discussed in Section 2.2 is split into the ServerPlatform, which is the platform running at the server of the telecommunication company, and the WebPlatform, which refers to another part of the platform that accesses the information about the n-th macro BS by TOC using a HyperText Markup Language (HTML) web page [46]. The WebPlatform is in HTML pages because it facilitates the development. The ServerPlatform receives information about the macro BS and stores all of them in a database. Also, the ServerPlatform controls the communication between WebPlatform and TOC. It is important to emphasize that the WebPlatform owns a user-friendly interface that allows visualizing the information and status of the energy sources, knowing the source being used by the macro BS and its status. Also, it works based on the easy management of information, which facilitates the visualization creation, edition, and deletion of the monitored variables.

The details of the development of the devices designed for this macro BS $\#n$ are as follows:

- **NetSensor** $\#n, i$: it is the i-th NetSensor device used in the n-th macro BS. This device is capable of monitoring and controlling the available energy sources (e.g., solar generation, wind generation, diesel generator, battery, and power utility). It is an essential element because it acquires information about energy sources using different kinds of sensors that can be connected to it. Also, due to the NetSensor devices are near to the SmartControl device, they receive commands from the DataConcentrator $\#n$ device to select the energy source that will feed the n-th macro BS and, with that,

the NetSensor devices enable or disable the SmartControl devices. The prototype of the NetSensor is shown in Figure 3. This device acquires the following information: Root Mean Square (RMS) AC Voltage, DC voltage level, diesel tank level, solar radiation, wind speed, and battery charging level.

- **DataConcentrator** $\#n$: it is the device used in the n-th macro BS. This device works as a local server for the macro BS $\#n$ and has an IP address used to connect to the ServerPlatform. The DataConcentrator $\#n$ is a device responsible for exchanging data and control messages with the NetSensors $\#n, i$. Also, it is responsible for sending the collected information to the ServerPlatform. Moreover, it is capable of storing information if the connection to the ServerPlatform is off. In addition, it manages the exchange of information between a macro BS $\#n$ and the ServerPlatform. A macro BS owns only one DataConcentrator device. Figure 4 shows the prototype of this device. Also, IoDataContrator device receive information from the NetSensor devices and feed a Mamdani T1FS [47]. This fuzzy system-based control is developed in the DataConcentrator device for performing the decision-making process for choosing an energy source to feed a macro BS. The design and details about the Mamdani T1FS are in Chapter 3.

- **SmartControl** $\#n, j$: it is the j-th control device used in the n-th macro BS. This device performs the switching among the available energy sources based on a decision sent by the n-th DataConcentrator device. This switching device is connected to an I/O interface of a NetSensor device.
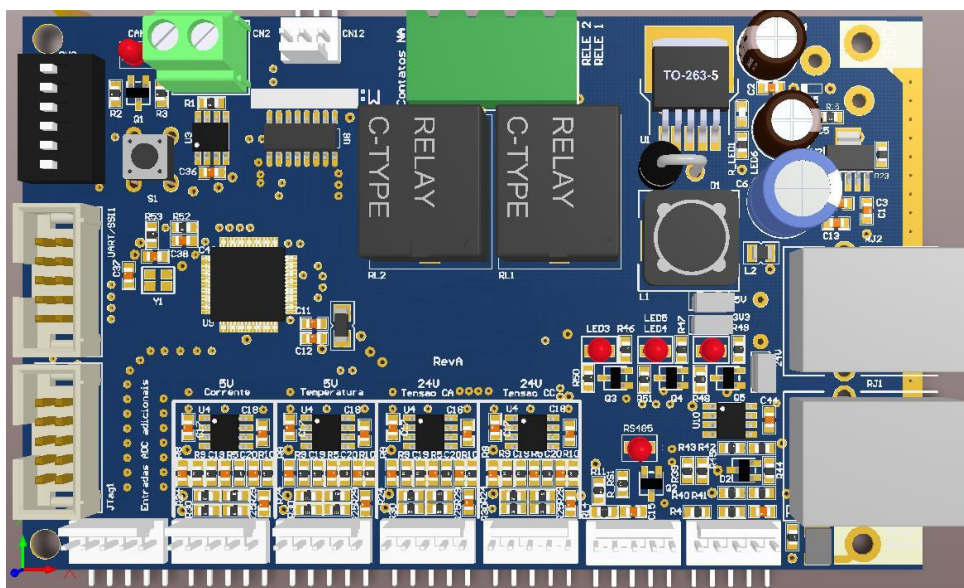
Figure 3 – The prototype of the NetSensor device.

Note that only one SmartControl device is used to coordinate the operation involving battery bank, solar generation, and wind generation. Power utility and diesel
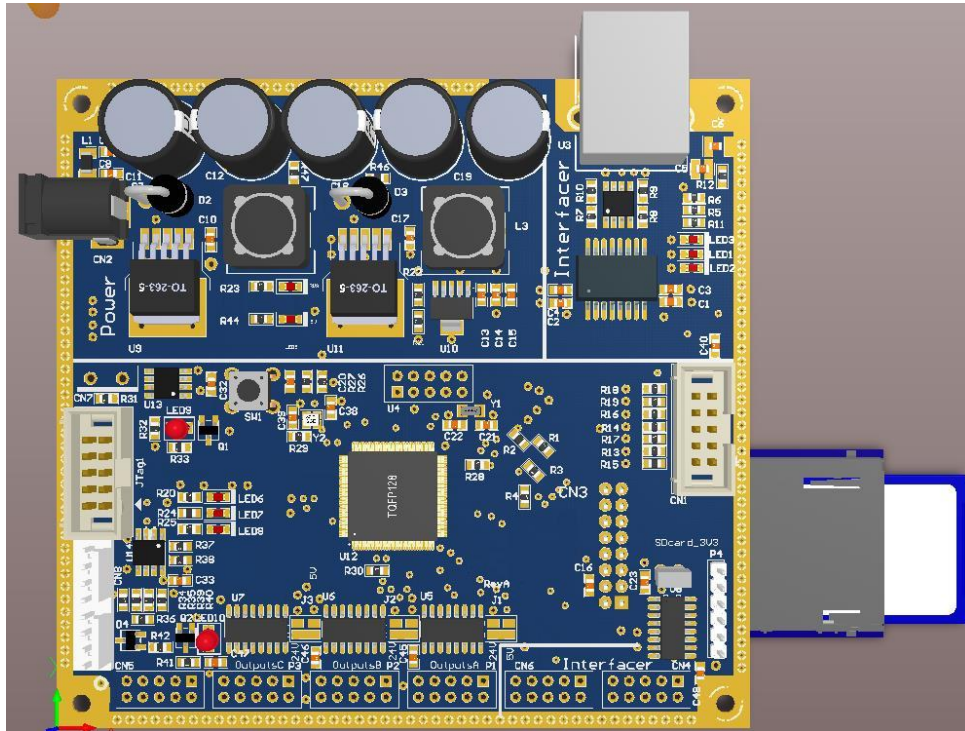
Figure 4 – The prototype of the DataConcentrator device.

generator are individually controlled by a dedicated SmartControl device. The rectification equipment works on the supplied energy by the power utility and the diesel generator. All types of equipment inside the macro BS are feed by a 48 V DC bus. Each source of energy makes use of one NetSensor device because it is designed to be a general-purpose device with several data acquisition channels and I/O interfaces for being used in a macro BS. Overall, the data collected by NetSensor devices are sent to the DataConcentrator device, which uses these information about energy sources to issue control commands to the SmartControl devices. The SmartControl devices are responsible for enabling or disabling the energy sources that will feed the macro BS $\#n$ and they are connected to I/O interfaces of the NetSensor devices.

The development of the feasible solution in a macro BS makes use of two types of data communication technologies. One of them is applied to connect all devices inside a macro BS, while the other deals with the data communication between a macro BS and the ServerPlatform. A brief description of these technologies is as follows:

- **Data exchanges among devices inside the macro BS $\#n$**: the operation of a macro BS yields electromagnetic disturbances that can disrupt the data communications among the existing devices inside a macro BS. In this regard, the use o wireless technology can decrease the energy reliability inside a macro BS. However, the use of a wireline technology to connect NetSensor devices to a DataConcentrator device is a simple solution to overcome the presence of electromagnetic disturbances inside

a macro BS. In this sense, in this development, all devices are connected by 8P8C connector through F/FTP Cat. 7 twisted pair cables, which are electromagnetic shielded [48]. Also, the data communications among devices make use of the Modbus Remote Terminal Unit (RTU) protocol [49]. The Modbus RTU is open-source and simple to develop. Other open-source or more sophisticated proprietary communication protocols could be used, such as IEC 61850, DNP3, Fieldbus, Profibus, DeviceNet [50] [51] [52] [53] [54]. However, for simplifying and optimizing the communication between NetSensor devices and DataConcentrator $\#n$, the Modbus RTU is used in the communication inside the macro BS.

- **Data exchanges between the macro BS $\#n$ and the ServerPlatform**: if a macro BS is located in an urban area, then a dedicated wireless/wireline can be used to connect a macro BS to the ServerPlatform, but the use of wireless technology can decrease the communication reliability between a macro BS and the ServerPlatform. Aiming to increase the communication reliability, the DataConcentrator device is connected to ServerPlatform by using an 8P8C connector through F/FTP Cat. 7 twisted pair cables, which are used to minimize electromagnetic interference [48]. The data communication between the DataConcentrator device and the ServerPlatform is based on the Modbus Transmission Control Protocol (TCP) protocol [49]. The Modbus TCP is chosen because it is open-source and simple to develop. Other open-source or more sophisticated proprietary communication protocols could be used, such as EthernetIP, Profinet, EtherCAT [55] [56] [57]. However, for simplifying and optimizing the communication between DataConcentrator and ServerPlatform, the Modbus TCP is used.

2.4 SUMMARY

This chapter discussed the problems of interruption of communications services suffered by telecommunications companies. In this regard, it discussed a feasible solution for BSs to deal with these problems. Also, it showed a development of the feasible solution applied to a macro BS.

3 THE CONTROL OF THE ENERGY SOURCES

The literature has shown that the increase of energy reliability in a BS relies on the availability of different energy sources because it is almost impossible to ensure that only one source can offer a high level of reliability. Giving a set of energy sources, one important issue to be taken into account is how to dynamically switch among them and, at the same time, to maximize the gains offered by their combination. In this regard, the switching has to be autonomous and based on the information gathered by sensors connected to the available energy sources in a way that the advantage offered by all available energy sources are suitably exploited. Regarding the choice of the energy source that will be used by the macro BS, the DataConcentrator and SmartControl are the devices responsible for performing the dynamic control of the available sources, see illustration of it in Fig. 2. The former device runs the algorithm responsible for choosing the energy source that will feed the macro BS while the latter performs the switching among the energy sources. Note that the switching actions are based on the information provided by the former to the latter devices.

There are different techniques for controlling the switching among the available energy sources in a macro BS. Among them, the use of the Mamdani T1FS [47] attracted the attention because the information about the available energy sources, such as power utility, solar generation, wind generation, diesel generator, and battery bank can be well modeled as linguistic terms. The information gathered from the energy sources can be physical quantities, such as temperature, current, voltage, wind speed, solar radiation, diesel tank level, battery charging level, among others. As a result, the power of a fuzzy system-based controller can be easily exploited to designed and updated the control strategy applied for switching the energy sources.

The T1FS is a well-establish theory that could be extended to cover higher levels of uncertainty such as Type-2 Fuzzy System (T2FS), which plays a significant role in these issues [58] [59]. However, this chapter discusses the use of the Mamdani T1FS for controlling the switching among different energy sources in the macro BS, which was presented in Section 2.3. This choice relies on the fact that the uncertainties related to the information obtained from the energy sources can be modeled by using type-1 membership functions. Mamdani T1FS is very appropriate to deal with engineering problems. Also, the use of the well-established Mamdani T1FS allows to come up with a solution that can be used as a benchmark in future research efforts toward this issue if higher levels of uncertainties are taken into account. In addition to the use of the Mamdani T1FS, centroid and height defuzzifiers are considered. The former is easy to design and demands high computational cost, while the latter is more difficult to design and demands low computational cost.

Given this context, this chapter is organized as follows: Section 3.1 discusses the Mamdani T1FS. Section 3.2 shows how to calculate the output of the Mamdani T1FS using the centroid defuzzifier. Section 3.3 presents the method to calculate the output of the Mamdani T1FS using the height defuzzifier. Section 3.4 addresses a brief summary of this chapter.

3.1 MAMDANI TYPE-1 FUZZY SYSTEM

The use of fuzzy system relies on the fact that fuzzy logic-based control tries to mimic the process performed by the human mind controlling actions. In this sense, this section describes the Mamdani T1FS, which is chosen to control the switching among the available energy sources [47]. This singleton T1FS makes use of Zadeh rules and Mamdani implication (i.e., product t-norm implication) with separable membership functions. Its adoption relies on the fact that input data is without uncertainty (e.g., is not corrupted by an additive noise) and there are not uncertainties associated with the membership functions for the antecedents and consequents. Also, the use of this fuzzy system is due to the simplicity for developing and updating its source code in the digital signal processor, which is part of the DataConcentrator device.

Based on the fact that the Mamdani T1FS needs to control several energy sources and the idea to use only one fuzzy system-based controller, which is similar to multiclassification problems handled by a single fuzzy system-based classifier in [60], Figure 5 shows the block diagram of the designed Mamdani T1FS, which is according with the idea portrayed in [60]. The main components of a fuzzy system are fuzzifier, rules, inference engine, and defuzzifier. According to Figure 5, the input vector $\mathbf{x} = \mathbf{x}'$ excites the Mamdani T1FS, where $\mathbf{x}'$ is a sample of the input vector. As a consequence, the outputs y_j ($j = 1, ..., Q$) are crisp values that depend on the $\mathbf{x}'$.
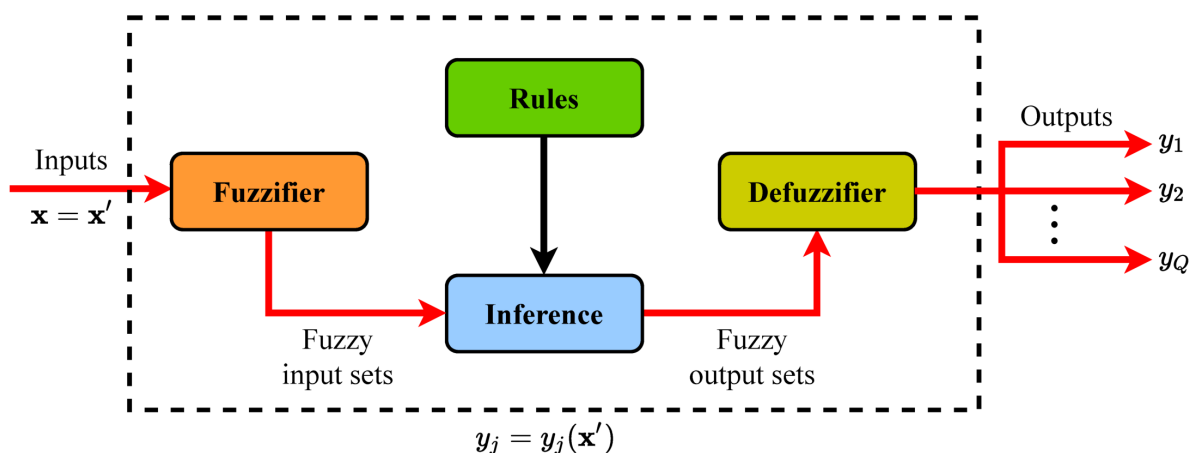
Figure 5 – A block diagram for the Mamdani T1FS.

Let the input vector $\mathbf{x} = [x_1, x_2, ..., x_P]^T \in X_1 \times X_2 \times ... \times X_P$, where P is the number of inputs and X_i is the universe of the discourse for x_i, be constituted by crisp information gathered from distinct energy sources and a battery bank. Also, assume the outputs $y_1 \in Y_1$, $y_2 \in Y_2$, ..., and $y_Q \in Y_Q$, respectively, where Q is the number of outputs and Y_j is the universe of the discourse for y_j. The outputs, which are crisp values, control the energy source for feeding the macro BS. In this sense, suppose that x_1 is described by V_{x_1} linguistic terms ($T_{x_1} = \{X_{1r}\}_{r=1}^{V_{x_1}}$), x_2 is described by V_{x_2} linguistic terms ($T_{x_2} = \{X_{2r}\}_{r=1}^{V_{x_2}}$), ..., and x_P is described by V_{x_P} linguistic terms ($T_{x_P} = \{X_{Pr}\}_{r=1}^{V_{x_P}}$). Also, suppose that y_1 is described by V_{y_1} linguistic terms ($T_{y_1} = \{Y_{1r}\}_{r=1}^{V_{y_1}}$), y_2 is described by V_{y_2} linguistic terms ($T_{y_2} = \{Y_{2r}\}_{r=1}^{V_{y_2}}$), ..., and y_Q is described by V_{y_Q} linguistic terms ($T_{y_Q} = \{Y_{Qr}\}_{r=1}^{V_{y_Q}}$). The structure of the l-th generic Zadeh type-1 first-order rule for a Mamdani T1FS is

$$R^l : \text{IF } x_1 \text{ is } F_1^l \text{ and } ... \text{ and } x_P \text{ is } F_P^l, \text{THEN } y_1 \text{ is } G_1^l \text{ and } ... \text{ and } y_Q \text{ is } G_Q^l, \qquad (3.1)$$

where $l = 1, ..., M$, $F_1^l \in T_{x_1}$, $F_2^l \in T_{x_2}$, ..., $F_P^l \in T_{x_P}$, $G_1^l \in T_{y_2}$, $G_2^l \in T_{y_2}$, ..., and $G_Q^l \in T_{y_Q}$. Also, F_i^l and G_j^l are type-1 fuzzy sets that are respectively denoted by $F_i^l = \{(x_i, \mu_{F_i^l}(x_i))|x_i \in X_i\}$ and $G_j^l = \{(y_j, \mu_{G_j^l}(y_j))|y_j \in Y_j\}$, where $\mu_{F_i^l}$ and $\mu_{G_j^l}$ are the membership functions for the inputs and outputs of the Mamdani T1FS, respectively.

The use of the Gaussian membership functions to represent the uncertainty associated with the l-rule for the i-th input and the j-th output are mathematically expressed as

$$\mu_{F_i^l}(x_i) = \exp\left[\frac{-(x_i - m_{F_i^l})^2}{2\sigma_{F_i^l}^2}\right] \qquad (3.2)$$

and

$$\mu_{G_j^l}(y_j) = \exp\left[\frac{-(y_j - m_{G_j^l})^2}{2\sigma_{G_j^l}^2}\right], \qquad (3.3)$$

respectively, where $m_{F_i^l}$ and $m_{G_j^l}$ are the center values of the membership functions, and $\sigma_{F_i^l}$ and $\sigma_{G_j^l}$ define the spread of the membership functions [61]. The Gaussian function is chosen because it presents a soft peak and it is less sensitive to the changes in crisp variables in comparison to the triangular kind of membership functions [61]. Also, it can be easily developed by using a lookup table.

The output of the inference engine, see Figure 5, presents the type-1 fuzzy output sets processed by type-1 fuzzy input sets and Zadeh rules of the Mamdani T1FS. This possessing uses t-norm (e.g., minimum, product) and/or t-conorm (e.g., maximum, algebraic sums) operators. Concerning the output of the Mamdani T1FS, two defuzzifiers are used to calculate the output y_j: the centroid defuzzifier and height defuzzifier. The goal of the defuzzifier is numerically quantify the processing of the fuzzy system converting

the type-1 fuzzy output sets into a real value $y_j \in Y_j$. Sections 3.2 and 3.3 present the mathematical formulation of these defuzzifiers.

3.2 CENTROID DEFUZZIFIER

This section presents the centroid defuzzifier to calculate the output of the Mamdani T1FS. With respect to a sample of the input vector $\mathbf{x}'$, the adoption of the centroid defuzzifier in the Mamdani T1FS results in the following output:

$$y_j(\mathbf{x}') = \frac{\sum_{n=1}^{N} y_{j_n} \mu_B(y_{j_n} \mid \mathbf{x}')}{\sum_{n=1}^{N} \mu_B(y_{j_n} \mid \mathbf{x}')}, \quad j = 1, \ldots, Q \tag{3.4}$$

where

$$\mu_B(y_{j_n} \mid \mathbf{x}') = \max_l \prod_{i=1}^{P} \mu_{F_i^l}(x_i') \star \mu_{G_j^l}(y_{j_n}) \tag{3.5}$$

is the output of the component inference in Figure 5 and it is composed of max-product operators associated with the values of x_i' in $\mu_{F_i^l}(x_i')$ and the output membership functions $\mu_{G_j^l}(y_j)$, P is the number of inputs and $\star$ is a product t-norm. According to (3.4), $\mu_B(y_j \mid \mathbf{x}')$ it is discretized at the N points, $y_{j_1} \in \mathcal{S}_j, \cdots, y_{j_N} \in \mathcal{S}_j$, where $\mathcal{S}_j$ is the support of $\mu_B(y_j \mid \mathbf{x}')$. Also, $y_j(\mathbf{x}')$ is shown as an explicit function of $\mathbf{x}'$ because $\mu_B(y_{j_n} \mid \mathbf{x}')$ is a function of the input $\mathbf{x}'$.

Overall, the centroid defuzzifier is not suggested when the Mamdani T1FS requires a real-time application and the hardware processing capacity is limited because it demands a huge computational complexity to calculate its output. The use of hardware with constraint over processing capacity characterizes the majority of new applications related to SG, the IoT, smart city and Industry 4.0 and it motivates the search for less complex fuzzy systems. That is the main reason for embracing the use of the height defuzzifier, which is described in Section 3.3. Finally, but not least, the design of the Mamdani T1FS based on the height defuzzifier takes advantage of *a priori* design of the one based on the centroid defuzzifier because the latter becomes a reference for designing the former.

3.3 HEIGHT DEFUZZIFIER

This section presents the height defuzzifier to calculate the output of the Mamdani T1FS. The height defuzzifier reduces the computational complexity of the Mamdani T1FS, but it is necessary to apply a training procedure to find the height defuzzifier parameters and make small adjustments in the antecedent parameters when the fuzzy system-based controller is *a priori* designed by a specialist. With respect to a sample of the input vector $\mathbf{x}'$, the output of the Mamdani T1FS with the height defuzzifier is given by [60]

$$y_j(\mathbf{x}') = \frac{\sum_{l=1}^{M} \theta_j^l \mu_B(y_j \mid \mathbf{x}')}{\sum_{l=1}^{M} \mu_B(y_j \mid \mathbf{x}')}, \quad j = 1, \ldots, Q, \tag{3.6}$$

where

$$\mu_B \left(y_j \mid \mathbf{x}' \right) = \prod_{i=1}^{P} \mu_{F_i^l}(x_i') \star \mu_{G_j^l}(y_j) \tag{3.7}$$

is the output of the component inference in Figure 5. It is composed of product t-norm operators associated with the values of x_i' in $\mu_{F_i^l}(x_i')$ and the output membership functions $\mu_{G_j^l}(y_j) = 1$, P is the number of inputs and $\star$ is a product t-norm. A matrix form for the output is given as follows:

$$\begin{aligned}
\mathbf{y}(\mathbf{x}') &= [y_1(\mathbf{x}'), y_2(\mathbf{x}'), \cdots, y_Q(\mathbf{x}')]^T \\
&= \boldsymbol{\Theta}\boldsymbol{\Phi}(\mathbf{x}'),
\end{aligned} \tag{3.8}$$

where

$$\boldsymbol{\Theta} = \begin{bmatrix} \theta_1^1 & \theta_1^2 & \cdots & \theta_1^M \\ \theta_2^1 & \theta_2^2 & \cdots & \theta_2^M \\ \vdots & \vdots & \ddots & \vdots \\ \theta_Q^1 & \theta_Q^2 & \cdots & \theta_Q^M \end{bmatrix}, \tag{3.9}$$

$$\boldsymbol{\Phi}(\mathbf{x}') = \begin{bmatrix} \phi_1(\mathbf{x}') & \phi_2(\mathbf{x}') & \cdots & \phi_M(\mathbf{x}') \end{bmatrix}^T, \tag{3.10}$$

and

$$\phi_l(\mathbf{x}') = \frac{\prod_{i=1}^{P} \mu_{F_i^l}(x_i')}{\sum_{l=1}^{M} \prod_{i=1}^{P} \mu_{F_i^l}(x_i')} \tag{3.11}$$

With that, $\mathbf{y}(\mathbf{x}') = [y_1(\mathbf{x}'), y_2(\mathbf{x}'), \cdots, y_Q(\mathbf{x}')]^T$ is an explicit function of $\mathbf{x}'$ because $\boldsymbol{\Phi}(\mathbf{x}')$ is a function of input of the Mamdani T1FS $\mathbf{x}'$, so, for each $\mathbf{x}'$ a different value is obtained for the output.

As stated earlier, the computational complexity using the height defuzzifier is reduced in comparison with the use of the centroid defuzzifier. This occurs because the height defuzzifier does not depend on the membership functions of the consequences because it assumes that $\mu_{G_j^l}(y_j) = 1$. Because of this, the number of numerical calculations is reduced in (3.8) and so it is necessary to calculate the $\boldsymbol{\Phi}(x')$ only once, while in (3.4) it is necessary to calculate NQ times the value of $\mu_B(y_{j_n} \mid \mathbf{x}')$ to obtain all outputs. On the other hand, the cost of reducing computational complexity is the training of the Mamdani T1FS to find the parameters that minimize the error rate in the output of the height defuzzifier. Among the types of training, this thesis uses a supervised training based on the steepest descent method, once the Mamdani T1FS uses input and output data that are already previously known. In this sense, Subsection 3.3.1 describes the supervised training based on the steepest descent method.

3.3.1 The supervised training

The supervised training of the Mamdani T1FS for the height defuzzifier can be accomplished by using an optimization method relying on the first-order or second-order information of the given cost function. In [60] was used the second-order information, which performs better than first-order information in terms of convergence speed but it is much more complex. On the other hand, the use of first-order information is more simple to develop and can offer excellent results when it is applied to perform adjustments of parameters when the fuzzy system-based controller is well-designed by a specialist [62]. Regarding first-order information for training fuzzy system-based controllers, the steepest descent method is very popular. According to [63], the adaptation of step-size in the use of the steepest descent method can remarkably increase the convergence speed of training procedure based on first-order information.

Giving the characteristics of the Mamdani T1FS-based controller with the centroid defuzzifier, the design of rule base and the membership functions for antecedents along with the supervised training are used for designing the Mamdani T1FS-based controller with the height defuzzifier. In this regard, the supervised training procedure based on the steepest descent method is adopted in this work. The steepest descent method is used to update the parameters of the membership functions of the antecedents and the parameters of the height defuzzifier.

Let us assume the use of a set of input-output pairs $(\mathbf{x}^{(k)} : \mathbf{y}^{(k)})$, where $\mathbf{y}^{(k)} = \left[y_1^{(k)}, y_2^{(k)}, ..., y_Q^{(k)} \right]^T$, $\mathbf{x}^{(k)} = \left[x_1^{(k)}, x_2^{(k)}, ..., x_P^{(k)} \right]^T$, where $k = 1, ..., L$ and L is the number of input-output pairs; the cost function can be denoted by [60]

$$J(\mathbf{w}^{(k)}) = \frac{1}{2} \sum_{j=1}^{Q} \left[y_j \left(\mathbf{x}^{(k)} \right) - y_j^{(k)} \right]^2 , \qquad (3.12)$$

where $y_j \left(\mathbf{x}^{(k)} \right)$ is the j-th output of the Mamdani T1FS-based controller, $y_j^{(k)}$ is the desired value for the j-th output, and $\mathbf{w}^{(k)}$ denotes the vector constituted by all parameters of the Mamdani T1FS controller, which is given by

$$\begin{aligned} \mathbf{w}^{(k)} = \quad & \left[m_{F_1^1}(k), \cdots, m_{F_P^1}(k), \cdots, m_{F_1^M}(k), \cdots, m_{F_P^M}(k), \right. \\ & \sigma_{F_1^1}(k), \cdots, \sigma_{F_P^1}(k), \cdots, \sigma_{F_1^M}(k), \cdots, \sigma_{F_P^M}(k), \\ & \left. \theta_1^1(k), \cdots, \theta_1^M(k), \cdots, \theta_Q^1(k), \cdots, \theta_Q^M(k) \right]^T . \end{aligned} \qquad (3.13)$$

Note that the goal of the supervised training method based on the steepest descent method is to minimize the error at the outputs of the Mamdani T1FS. To do this, the antecedents parameters $\mu_{F_i^l}(k)$ and $\sigma_{F_i^l}(k)$, and the height defuzzifier parameters $\theta_j^l(k)$ are adjusted.

Based on (3.12), the gradient vector $J(\mathbf{w}^{(k)})$ is expressed as

$$
\nabla J(\mathbf{w}^{(k)}) = \left[\frac{\partial J(\mathbf{w}^{(k)})}{\partial m_{F_1^1}(k)}, \cdots, \frac{\partial J(\mathbf{w}^{(k)})}{\partial m_{F_P^1}(k)}, \cdots, \frac{\partial J(\mathbf{w}^{(k)})}{\partial m_{F_1^M}(k)}, \cdots, \frac{\partial J(\mathbf{w}^{(k)})}{\partial m_{F_P^M}(k)}, \right.
$$
$$
\frac{\partial J(\mathbf{w}^{(k)})}{\partial \sigma_{F_1^1}(k)}, \cdots, \frac{\partial J(\mathbf{w}^{(k)})}{\partial \sigma_{F_P^1}(k)}, \cdots, \frac{\partial J(\mathbf{w}^{(k)})}{\partial \sigma_{F_1^M}(k)}, \cdots, \frac{\partial J(\mathbf{w}^{(k)})}{\partial \sigma_{F_P^M}(k)},
$$
$$
\left. \frac{\partial J(\mathbf{w}^{(k)})}{\partial \theta_1^1(k)}, \cdots, \frac{\partial J(\mathbf{w}^{(k)})}{\partial \theta_1^M(k)}, \cdots, \frac{\partial J(\mathbf{w}^{(k)})}{\partial \theta_Q^1(k)}, \cdots, \frac{\partial J(\mathbf{w}^{(k)})}{\partial \theta_Q^M(k)} \right]^T , \quad (3.14)
$$

in which the derivatives of $J(\mathbf{w}^{(k)})$ with respect to the parameters $m_{F_i^l}(k)$, $\sigma_{F_i^l}(k)$, and $\theta_j^l(k)$, are given by

$$
\frac{\partial J(\mathbf{w}^{(k)})}{\partial m_{F_i^l}(k)} = \sum_{j=1}^{Q} \left\{ \left[y_j(\mathbf{x}^{(k)}) - y_j^{(k)} \right] \left[\theta_j^l(k) - y_j(\mathbf{x}^{(k)}) \right] \right\} \left[\frac{x_i^{(k)} - m_{F_i^l}(k)}{\sigma_{F_i^l}^2(k)} \right] \phi_l \left(\mathbf{x}^{(k)} \right) , \quad (3.15)
$$

$$
\frac{\partial J(\mathbf{w}^{(k)})}{\partial \sigma_{F_i^l}(k)} = \sum_{j=1}^{Q} \left\{ \left[y_j(\mathbf{x}^{(k)}) - y_j^{(k)} \right] \left[\theta_j^l(k) - y_j(\mathbf{x}^{(k)}) \right] \right\} \left[\frac{\left(x_i^{(k)} - m_{F_i^l}(k) \right)^2}{\sigma_{F_i^l}^3(k)} \right] \phi_l \left(\mathbf{x}^{(k)} \right) ,
$$
$$
(3.16)
$$

and

$$
\frac{\partial J(\mathbf{w}^{(k)})}{\partial \theta_j^l(k)} = \left[y_j(\mathbf{x}^{(k)}) - y_j^{(k)} \right] \phi_l \left(\mathbf{x}^{(k)} \right) \quad (3.17)
$$

respectively. The steepest descent method only updates the parameter $m_{F_i^l}(k)$, $\sigma_{F_i^l}(k)$ and $\theta_j^l(k)$ one time for each $J(\mathbf{w}^{(k)})$ and it has the following structure:

$$
m_{F_i^l}(k+1) = m_{F_i^l}(k) - \beta \frac{\partial J(\mathbf{w}^{(k)})}{\partial m_{F_i^l}(k)}, \quad (3.18)
$$

$$
\sigma_{F_i^l}(k+1) = \sigma_{F_i^l}(k) - \beta \frac{\partial J(\mathbf{w}^{(k)})}{\partial \sigma_{F_i^l}(k)} \quad (3.19)
$$

and

$$
\theta_j^l(k+1) = \theta_j^l(k) - \beta \frac{\partial J(\mathbf{w}^{(k)})}{\partial \theta_j^l(k)}, \quad (3.20)
$$

where $\beta \in \mathbb{R} | 0 < \beta < 1$ is the step-size or the learning parameter.

3.4 SUMMARY

This chapter focused on the control switching among the energy sources in the macro BS. In this sense, this chapter used the Mamdani T1FS and showed two approaches to calculate the output of the Mamdani T1FS. The former was the centroid defuzzifier,

which is easy to develop and has a high computational complexity, the latter was the height defuzzifier, which is most difficult to develop and presents reduced computational complexity.

4 MACRO BS POWER AND ENERGY SOURCES MODELS

The unavailability of data services by telecommunications companies is a serious problem and must be treated with attention since it is considered an essential service. These data services are made available using BSs, which can be on-grid or off-grid BSs. Generally, in urban areas, it is most common to find on-grid BSs. In rural areas, off-grid BSs are most common because they are located in isolated places. In relation to the problem of the unavailability of data services by telecommunications companies, the power outage has a significant weight in these occurrences. This problem can be mitigated by increasing the number of energy sources available to feed a BSs (e.g., power utility, solar generation, wind generation, diesel generator) and using a battery bank to backup the energy taken from the renewable sources. In this sense, it is important to come up with a tool to evaluate how reliable is the set of energy sources in BSs.

Given this context, this chapter describes the power model of a macro BS, which consists of a fixed part and another that varies according to the transmission power. Also, it briefly details the mathematical formulations related to energy sources and the battery bank used in the macro BS, which was presented in Section 2.3. The information about the energy sources are taken considering the weather data for a possible macro BS located in the city of Juiz de Fora, Brazil. Also, the wind speed and solar radiation data sets are according to the database [64] of the Brazilian National Institute of Meteorology and they are used to design the solar generation and wind generation. Moreover, this chapter addresses a method based on the reliability function for providing a statistical quantification of the energy reliability in a macro BS for a given set of sources of energy.

This chapter is organized as follows: Section 4.1 presents the power model for a macro BS. Section 4.2 presents the information about the power utility used in the city of Juiz de Fora. Section 4.3 discusses the daily energy generated by solar generation. Section 4.4 addresses the daily energy generated by wind generation. Section 4.5 shows the information about diesel generator. Section 4.6 describes how to design a battery bank using a set of battery packs. Section 4.7 addresses the use of the reliability function for a statistical quantification of the energy reliability in a macro BS. Finally, Section 4.8 summarizes this chapter.

4.1 POWER MODEL FOR MACRO BS

According to [16], the power consumption in a macro BS varies with the traffic load over time. In this regard, the relationship between the power consumption of a macro BS, P_{in}, and the relative RF output power, P_{out}, considering the number of

transmitting/receiving antennas, $N_{TRX} \in \mathbb{N}_+$, can be expressed as

$$P_{\text{in}} = \begin{cases} N_{TRX}(P_0 + \Delta_p P_{\text{out}}) & , \ 0 < P_{\text{out}} \leqslant P_{\text{max}} \\ N_{TRX} P_{\text{sleep}} & , \ P_{\text{out}} = 0, \end{cases} \tag{4.1}$$

where P_0 denotes the power consumption at the zero RF output power P_{out}, Δ_p is the slope of the load-dependent power consumption and P_{max} denotes the maximum RF output power at maximum load. Also, sleep mode power consumption, P_{sleep}, refers to the period of time in which macro BS is not transmitting or receiving data.

This thesis uses the power data of an LTE macro BS measured in the field by [19]. This macro BS has a number of transmitting/receiving antennas equal to $N_{TRX} = 6$ (i.e., 3 sectors with 2 antennas) and power given by $P_{\text{in}} = 772.907 + 1.214P_{\text{out}}$, where P_{out} ranges from $[0, 40]$ W. This thesis inserts this macro BS into the feasible solution presented in Chapter 2. In this sense, the power consumed by macro BS is approximately delimited by the interval $[773, 822]$ W. Also, this macro BS makes use of 48 V bus for feeding its devices and its daily energy consumption is 19.7 kWh at full data traffic load and minimum of 18.6 kWh without data traffic load [19]. Moreover, the use of an air conditioner adds a daily energy consumption of 18 kWh [65]. As a result, the daily energy consumption in the macro BS fluctuates from the minimum 36.7 kWh for no traffic load and the maximum 37.8 kWh for the full data traffic load. This means that the average energy and power consumption in the macro BS are equal to $E_{\text{avg}} = 37.3$ kWh and $P_{\text{avg}} = 1552$ W, respectively.

4.2 POWER UTILITY

Power utility is the energy source that supplies electrical energy using RMS AC for macro BS. This is the main source of energy for the macro BS, discussed in Section 2.3, when it is located in the urban area. In Brazil, the mains frequency is equal to 60 Hz and there are different RMS AC voltage values for low-voltage electric power grids, such as 220/127 V, 380/220 V, 440/220 V, in different parts of the country. In the city of Juiz de Fora, the energy delivered by the local power utility makes use of RMS AC 127/220 V in the low-voltage and outdoor power distribution networks, which is adopted in this thesis.

4.3 SOLAR GENERATION

The solar power produced by a solar panel, in terms of kW, is expressed as [66]

$$P_{\text{sun}} = \eta \gamma A I \ \ (\text{kW}), \tag{4.2}$$

where A denotes the area occupied by the solar panel in square metre (m^2); I denotes the solar radiation in kilowatt per square metre (kW/m^2); η the photo-voltaic module efficiency, and γ (taken as 0.75) the performance ratio or the coefficient of losses. Both η

and γ are dimensionless quantities. In this regard, the average daily solar energy produced by a solar panel, in terms of kWh, can be calculated as [66]

$$E_{\text{sun, daily}} = \eta \gamma A I_{\text{daily}} \quad (\text{kWh}), \tag{4.3}$$

where I_{daily} denotes the average daily solar radiation in kilowatt-hora per square metre (kWh/m^2).
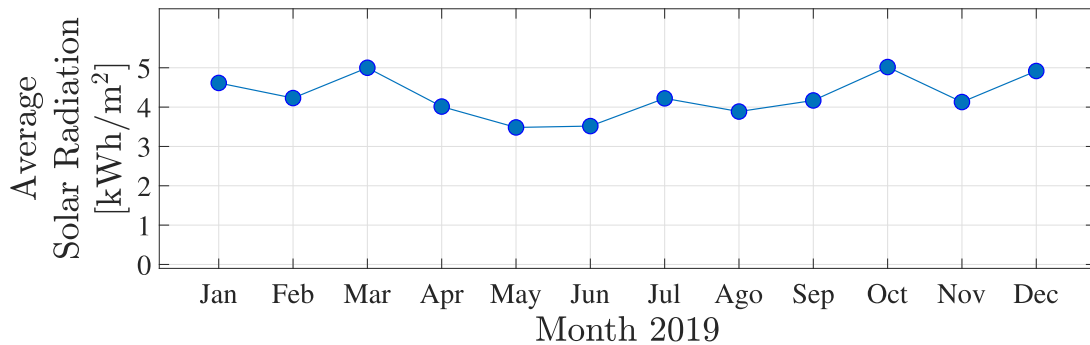
Figure 6 – The average daily solar radiation in each month of 2019, in the city of Juiz de fora, Brazil.

According to the database [64] of the Brazilian National Institute of Meteorology, the average daily solar radiation for each month during the year of 2019, in the city of Juiz de Fora, is shown in Figure 6. Note that the lowest and the highest average values occurred in May (3.5 kWh/m^2) and October (5.0 kWh/m^2), respectively.
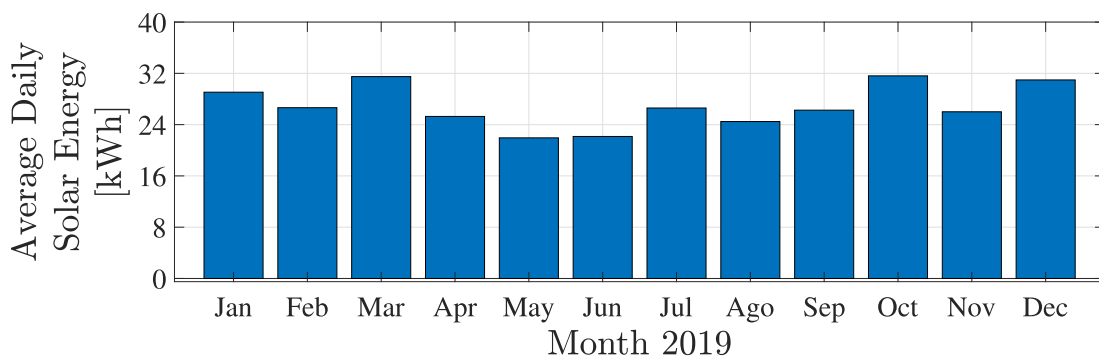
Figure 7 – The average daily solar energy generation in the year of 2019.

In this regard, the solar generation is designed with thirty 280 W - Yingli YL280P-29B photovoltaic solar panels [67]. Each solar panel has 1.64 m^2 of area (A), 17.1% of module efficiency (η_m), and 0.75 of coefficient of losses (γ). Figure 7 shows the average daily solar energy for all months of 2019 in the city of Juiz de Fora, Brazil. This quantity

ranges between 22 kWh and 32 kWh. Based on the provided information, the minimum average daily radiation (I_{daily}) of 3.48 kWh/m^2 occurs in May and, as a consequence, the average daily solar energy generated ($E_{\text{sun, daily}}$) of these thirty 1.64 m^2 panels is around 22 kWh. On the other hand, the maximum average daily solar energy is generated in October and, as a consequence, an average daily solar energy of 32 kWh is generated.

4.4   WIND GENERATION

Different from the Sun, the wind is available all daylight and night. A disadvantage is that the wind speed may be random because it heavily depends upon the weather conditions. This thesis uses the data set of the database [64] of the Brazilian National Institute of Meteorology for designing the wind generation. This data set is related to wind speed (m/s) in the city of Juiz de Fora, Brazil, for the year 2019.

Regarding the wind speed data of the Brazilian National Institute of Meteorology, they were extracted at an elevation of $h_{\text{ref}} = 10$ m, but wind turbines are usually installed at a higher elevation. In this regard, the wind speed data need to be corrected to account for this difference. In this sense, the wind speed (v) is calculated as [68]

$$v = v_{\text{ref}} \frac{\ln(h/z_0)}{\ln(h_{\text{ref}}/z_0)}, \tag{4.4}$$

where v_{ref} is the wind speed (m/s) on the elevation site h_{ref}, z_0 is the roughness site in metre (taken as 0.7 m) [69], and h is the new site elevation in metre.

There are three different methods for calculating the energy produced by a wind turbine [66]. The adopted method in this thesis refers to the use of the *two*-parameter Weibull Probability Density Function (PDF) to model the wind speed V (m/s) as a Random Variable (RV) and the power curve provided by the wind turbine manufacturer. This method is adopted due to its simplicity of application when previous data set is available. The *two*-parameter Weibull PDF is given by [70] [71]

$$f_V(v) = \frac{k}{\lambda} \left(\frac{v}{\lambda} \right)^{k-1} e^{-\left(\frac{v}{\lambda} \right)^k}, \tag{4.5}$$

where k is the shape parameter and λ the scale parameter. These parameters are expressed as

$$k = \left(\frac{\sigma}{\mu} \right)^{-1.086} \tag{4.6}$$

and

$$\lambda = \frac{\mu}{\Gamma \left(1 + \frac{1}{k} \right)} \tag{4.7}$$

where $\Gamma(.)$ is the gamma function, σ is the standard deviation and μ is the average wind speed of the RV.

According to the database of the Brazilian National Institute of Meteorology and considering the site elevation of $h = 100$ m, the average wind speed (m/s) in the city of Juiz de Fora for each month of the year 2019 is shown in Figure 8 [64]. The lowest and highest average values occurred in May (4.0 m/s) and November (5.6 m/s), respectively. In this sense, Figure 9 shows the PDF of the wind speed RV V in site elevation of 100 m for January 2019 ($k = 2.09$ and $\lambda = 5.22$). Also, each month of 2019 uses a Weibull PDF curve similar to the one presented for January in Figure 9.
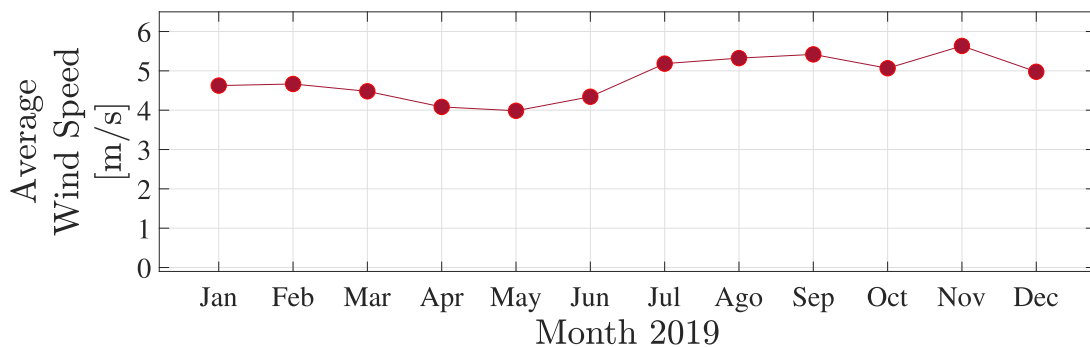
Figure 8 – The average wind speed in each month of 2019, in the city of Juiz de Fora, Brazil.
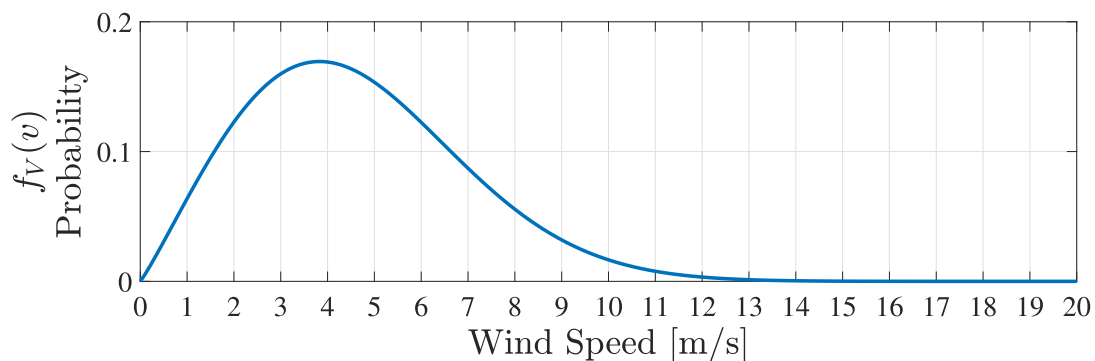
Figure 9 – The Weibull PDF of the wind speed random variable in January 2019.

Regarding the wind turbine, this thesis uses the Bergey BWC Excel 10, which has a maximum power of 10 kW for a wind speed of 14 m/s. Figure 10 shows its power curve [72] as a function of wind speed. Due to large variations in wind speed, a wind turbine operates at the maximum power for a low percentile how Figure 9 illustrates. Given the wind speed statistical model and the power curve of a wind turbine, the average daily energy produced, in each month of the year, is expressed as [73]

$$E_{\text{wind,daily}} = \Delta t \int_0^\infty P(v) f_V(v) \, dv, \tag{4.8}$$

where $P(v)$ is the power curve of the wind turbine given by the manufacturer, $f_V(v)$ is the Weibull PDF for the corresponding month and Δt is the time interval in hours (24 h in this case).
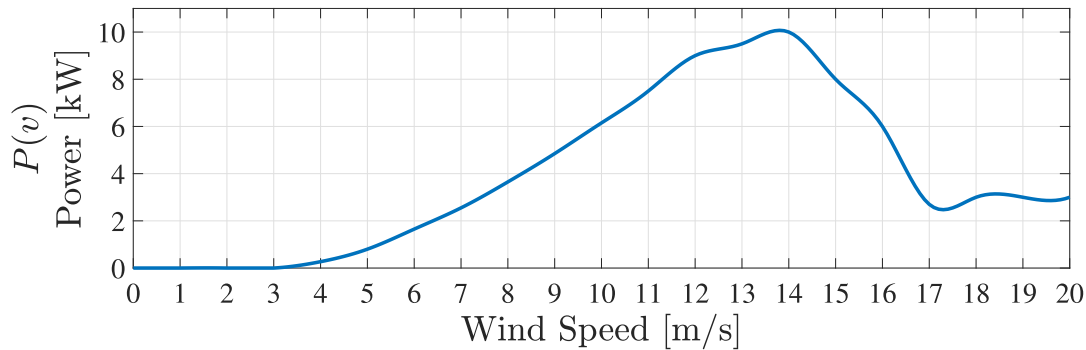
Figure 10 – The power curve of the Bergey BWC Excel 10 wind turbine.

In this regard, the use of the Bergey BWC Excel 10 wind turbine at the wind generation results in the average daily wind energy ($E_{\text{wind,daily}}$) in each month of 2019 in the city of Juiz de Fora as shown in Figure 11. In this plot, the values of $E_{\text{wind,daily}}$ ranges from 16 kWh and 46 kWh.
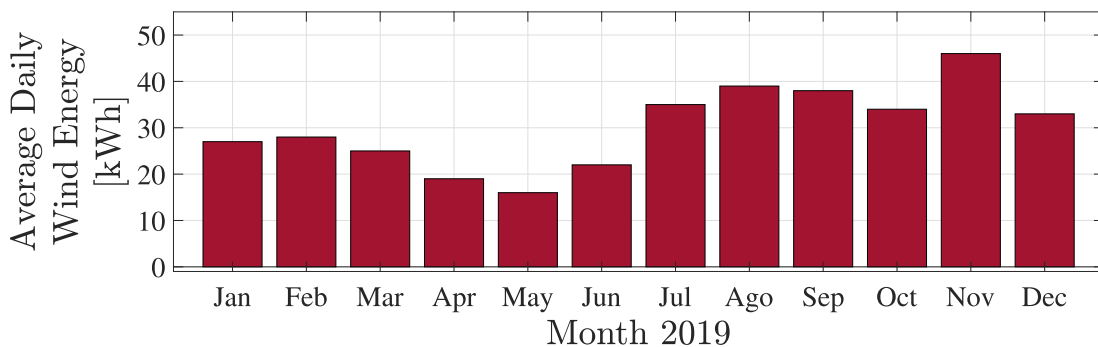
Figure 11 – The average daily wind energy generation in the year of 2019.

4.5 DIESEL GENERATOR

The generation of electrical energy with a diesel-based machine is used when no other energy source is available because it is the most expensive source of energy. Giving the macro BS power, this thesis adopts the Toyama TD7000CX3ED RMS AC 220 V/60 Hz diesel generator [74]. This diesel generator has a fuel backup in the diesel tank of 15.0 liters (L) and an autonomy of 7.1 hours (h) in the rated power (4400 W). It is assumed that the power produced by the diesel generator is in the interval [1527, 1576] W, which corresponds

to an autonomy between $7.1 \times 4400/1576 = 19.8$ h and $7.1 \times 4400/1527 = 20.5$ h for the macro BS. Also, it is important to emphasize that the consumption of the diesel generator varies between $15.0/20.5 = 0.73$ L/h and $15.0/19.8 = 0.76$ L/h when it is turned on. Figure 12 shows a photo of the chosen diesel generator.

Figure 12 – The diesel generator Toyama TD7000CX3ED.

4.6 BATTERY

A battery bank can be used to generate an energy backup to feed the macro BS during a time interval in which the energy sources are not generating electrical energy. In this sense, it can be used to store energy produced by renewable sources (solar and wind) and to be used to reduces the cost with energy consumption of the power utility. In this regard, a battery bank is used by a macro BS to increase energy reliability. The cost of a battery bank considerably increases with its storage capacity increases. For assessing the size of the battery bank, it is mandatory to consider the load power consumption and for how long it will be feed by the battery bank.

Giving a conservative perspective, the batteries should not be discharged below 50% of their maximum charging level in order to preserve their lifetime. Therefore, from a practical perspective, the battery bank must be specified with a storage capacity corresponding to twice the energy consumption of the load. This practical approach ensures that the lifetime will be extended by avoiding excessive discharging. In fact, if discharged below a certain level, the lifetime of a battery quickly deteriorates. In this sense, the energy backup in Ampere.hora (Ah) of the battery bank, E_{bb}, can be described as

$$E_{bb} = 2\frac{P_{\text{avg}}\Delta t}{V}, \tag{4.9}$$

where P_{avg} is the average power in Watt consumed by the macro BS, Δt is the time interval for backup, which is given in hour (e.g., 10h, 12h, and 24h), and V is the DC voltage used in the macro BS. The multiplication by 2 in (4.9) is used to ensure that twice the required energy backup is available, which is a conservative approach recommended by industry to deal with in real situations. Also, the number of battery packs, N_{bp}, used in a battery bank is given by

$$N_{bp} = \left\lceil \frac{E_{bb}}{E_{bp}} \right\rceil, \tag{4.10}$$

where E_{bp} is the energy backup in a single battery pack in Ah and $\lceil x \rceil = \min\{n \in \mathbb{Z} \mid n \geq x\}$.

Aiming to store the yielded solar and wind energies, this thesis uses Changhong CH48100 LiFePO battery packs ($V = 48$ V, $E_{bp} = 100$ Ah) connected in parallel for storing the energy yielded by the solar generation and wind generation [75]. This battery pack is an interesting choice because its service life exceeds 3000 cycles, which represents a lifetime longer than ten years.

Given the information about the power model of a macro BS, and the energy sources and battery bank used for feeding the macro BS presented in this chapter, Section 4.7 addresses a probabilistic model to quantify the energy reliability in a macro BS.

4.7 THE ENERGY RELIABILITY ANALYSIS

This section addresses the use of the system reliability theory for providing a statistical quantification of the energy reliability in a macro BS under the availability of a set of energy sources. The system reliability theory has been widely and successfully applied in different areas of knowledge, such as risk and safety analysis, quality, maintenance optimization, environmental protection, engineering design [76]. Based on well-established results, the reliability function is, for the first time, applied to evaluate the energy reliability in a macro BS.

In this regard, consider t_0 the instant when a fail occurs in the main energy source (e.g., power utility for on-grid macro BS) and t_1 when the telecommunication service of the macro BS becomes unavailable considering that the other set of energy sources (e.g., the use of wind generation, solar generation, battery bank or diesel generator) are available for feeding the macro BS. This unavailable of the service is due to the occurrence of the power outage in the macro BS. In this sense, the time interval $t = t_1 - t_0$ is the Time to Power Outage (TTPO). Note that TTPOs values can be interpreted as samples of an RV. This RV can be modeled with a *three*-parameter Weibull PDF [76], because this PDF is very flexible, and can, through an appropriate choice of parameters, model many types

of fail rate behaviors [76]. The Weibull PDF is one of the most widely used in reliability analysis.

Regarding the RV TTPO, the *three*-parameter Weibull PDF of this RV is expressed as

$$f(t) = \begin{cases} 0 & , \ 0 \leqslant t \leqslant \xi \\ \frac{k}{\lambda} \left(\frac{t-\xi}{\lambda} \right)^{(k-1)} \exp\left\{ - \left[\frac{(t-\xi)}{\lambda} \right]^k \right\} & , \ t > \xi, \end{cases} \tag{4.11}$$

where t is the time interval or TTPO in hour, k is the shape parameter, λ is the scale parameter and ξ is the location parameter. Also[1],

$$k = \left(\frac{\sigma_t}{\mu_t} \right)^{-1.086} \tag{4.12}$$

and

$$\lambda = \frac{\mu_t - \xi}{\Gamma\left(1 + \frac{1}{k}\right)}, \tag{4.13}$$

where $\Gamma(.)$ is the gamma function, σ_t is the standard deviation of the RV TTPO and μ_t is the Mean of Time to Power Outages (MTTPO) value. As a result, the energy reliability function is expressed as

$$R(t) = 1 - F(t) = \begin{cases} 1 & , \ 0 \leqslant t \leqslant \xi \\ \exp\left[- \left(\frac{t-\xi}{\lambda} \right)^k \right] & , \ t > \xi, \end{cases} \tag{4.14}$$

where $F(t) = \int_{-\infty}^{t} f(\alpha)d\alpha$ is the cumulative distribution function and $f(t)$ is the PDF given by (4.11).

4.8   SUMMARY

This chapter presented the power model for a macro BS. Also, it described the use of the power utility, solar generation, wind generation, and diesel generator in the development of the feasible solution of the macro BS. Moreover, it detailed how to calculate the battery bank using a set of battery packs. Lastly, this chapter addressed the reliability function for providing a probabilistic model to quantify the energy reliability in a macro BS for a given set of sources of energy.

---

[1]   Equations (4.12) and (4.13) are applied for *three*-parameter Weibull PDF and they are similar to Equations (4.6) and (4.7) that are applied for *two*-parameter Weibull PDF.

5 NUMERICAL RESULTS

This chapter discusses numerical analyses related to the energy reliability of the macro BS, which was detailed in Section 2.3, when power utility, a diesel generator, a solar generation, a wind generation, and a battery bank, which were described in Chapter 4, are jointly combined, in distinct manners, to improve the energy reliability in the macro BS. Moreover, it numerically evaluates and analyzes the use of the Mamdani T1FS with centroid and height defuzzifiers for managing the switching among the sources of energy in the macro BS, under different scenarios. Note that the chosen scenarios illustrate representative operational conditions; however, other scenarios can be easily built to carry out new analyses.

To offer a systematic presentation of the numerical analyses, this chapter is organized as follows: Section 5.1 describes the data sets used in the numerical simulations and the delimited boundaries to define representative simulations scenarios. Section 5.2 shows the designed Mamdani T1FS with the centroid defuzzifier. In the sequel, Subsection 5.2.1 presents the controlling actions performed by the Mamdani T1FS and illustrates the time interval that the macro BS experiences a power outage after to occur a fail in the power utility. Subsection 5.2.2 analyzes the energy reliability in scenarios that covering different amounts of fuel backup in the diesel tank, energy backup in the battery bank, and the set of available energy sources in a macro BS. Finally, Section 5.3 discusses the performance using the Mamdani T1FS with the height defuzzifier in comparison to the one based on the centroid defuzzifier.

5.1 SIMULATION DESCRIPTIONS

Aiming to carry out numerical simulations, the daily energy and power consumption in the macro BS are modeled as a continuous and uniform RVs in the interval delimited by $[36.7, 37.8]$ kWh and $[1527, 1576]$ W, respectively. The average values of energy and power consumption RVs are given by $E_{avg} = 37.3$ kWh and $P_{avg} = 1552$ W, respectively. Also, the sources of energy used in the simulations for feeding the macro BS are power utility, solar generation, wind generation, and diesel generator, in addition to the battery bank used to generate energy backup.

Regarding Chapter 4, the power utility, which operates with RMS AC 220 V/60 Hz, is capable of feeding a macro BS while it is in normal operation. Also, the diesel generator offers RMS AC 220 V/60 Hz and its feeding capacity is delimited by the fuel backup (i.e., the amount of fuel in the diesel tank). The diesel tank level is modeled as a continuous and uniform RV that is defined in the interval $[0, D]$ L, where D denotes the maximum fuel backup for the diesel generator. In this regard, two different fuel backups will be used for the diesel generator, 15.0 L and 30 L. Also, how it was discussed in Chapter 4, the fuel

consumption per hour of the diesel generator ranges from 0.73 L/h up to 0.76 L/h when it is turned on.

The use of the solar and wind generations in the numerical simulations also agree with Chapter 4. In this regard, it is valuable to show the summation of the average energies daily generated by solar generation and wind generation in the months of 2019, see details in Chapter 4. This summation is shown in Figure 13, in which it is clear that average daily generated energy surpasses the average daily demand of a macro BS ($E_{\mathrm{avg}} = 37.3$ kWh).
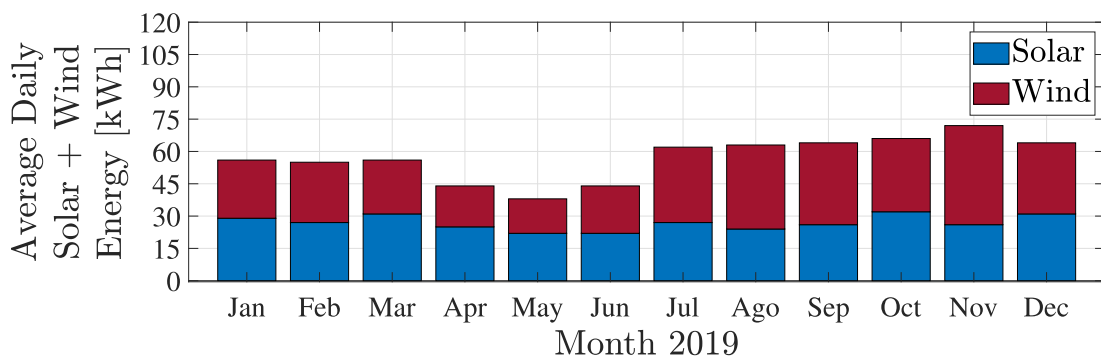
Figure 13 – The summation of the average energy daily generated by solar generation and wind generation in the year of 2019.

Concerning the battery bank, the simulation assume three different time backups (Δt) in the simulations: 24 h, 12 h, and 10 h. These three values of Δt are associated with battery banks of $E_{bb} = 1552$ Ah, $E_{bb} = 776$ Ah, and $E_{bb} = 647$ Ah, respectively. According to (4.9) and (4.10), these values of E_{bb} demands 16, 8, and 7 battery packs (N_{bp}) to make up the battery banks, respectively. The battery banks with 16, 8, and 7 battery packs may offer energy backups (B) of 76.8 kWh, 38.4 kWh, and 33.6 kWh, respectively. In this regard, during the simulations, the initial energy backup in the each battery bank is modeled as continuous and uniform RV that is defined in the interval $[0.9B, B]$ kWh. Finally, the recharging of the battery bank is done according to solar generation using solar power P_{sun} described by (4.2) and wind generation according to its power curve $P(v)$ how discussed in Section 4.4. Also, the power provided by the battery bank to the macro BS is given by $P_{\mathrm{bat}} = P_{\mathrm{in}} \mid P_{\mathrm{in}} \in [1527, 1576]$ W

Overall, the adoption of two fuel backups for the diesel generator and three configurations of energy backup in the battery bank results in $U = 6$ different configurations for evaluation. Note that each configuration demands a specific design of the Mamdani T1FS because each of them covers a different combination of energy sources and battery banks. Each configuration is shortly described as follows:

- Configuration #1: $B = 76.8$ kWh and $D = 30$ L.

- Configuration #2: $B = 38.4$ kWh and $D = 30$ L.

- Configuration #3: $B = 33.6$ kWh and $D = 30$ L.

- Configuration #4: $B = 76.8$ kWh and $D = 15$ L.

- Configuration #5: $B = 38.4$ kWh and $D = 15$ L.

- Configuration #6: $B = 33.6$ kWh and $D = 15$ L.

Giving these boundaries to carry out the numerical simulations, $V = 7$ scenarios are defined to characterize typical faulty conditions of a macro BS, in which the power utility fails (i.e., stop to feed the macro BS). A short description of each of them is provided as follows:

- Scenario #1: if the power utility fails, then diesel generator, solar generation, wind generation, and battery bank are available.

- Scenario #2: if the power utility fails, then diesel generator, solar generation, and battery bank are available.

- Scenario #3: if the power utility fails, then diesel generator, wind generation, and battery bank are available.

- Scenario #4: if the power utility fails, then solar generation, wind generation, and battery bank are available.

- Scenario #5: if the power utility fails, then solar generation, and battery bank are available.

- Scenario #6: if the power utility fails, then wind generation, and the battery bank are available.

- Scenario #7: if the power utility fails, then diesel generator, and battery bank are available.

5.2 MAMDANI TYPE-1 FUZZY SYSTEM USING CENTROID DEFUZZIFIER

Concerning the information about simulation descriptions presented in Section 5.1, for each configuration $\#u \mid u = 1, ..., 6$, a Mamdani T1FS using centroid defuzzifier is developed. Each Mamdani T1FS is designed with five inputs, x_1 to x_5, and three outputs, y_1 to y_3. The variables x_1 to x_5 correspond to the following information provided by NetSensor devices: the RMS AC voltage of the power utility (x_1), the diesel tank fuel level (x_2), the solar radiation (x_3), the wind speed (x_4), and the battery charging level (x_5). It is important to emphasize that the Mamdani T1FS can make use of sensing information

together with other ones, such as the price of oil, the price of electric energy, time of day within a linguistic perspective to achieve improved performance; however, only sensing information gathered from the energy sources and storage are considered in the numerical simulations. Note that the variables $y_j \in \mathbb{R} \mid j = 1, 2, 3$ are the outputs of the Mamdani T1FS. In the sequel, a decision-maker selects the current energy source for feeding the macro BS. It chooses y_j showing the highest value and, as a consequence, it set the output $y_{d_j} = 1$ and the others $y_{d_r} = 0$ ($r \neq j \mid j, r = 1, 2, 3$). The outputs of the decision-maker $y_{d_j} \in \{0, 1\} \mid j = 1, 2, 3$ are sent to the SmartControl devices $\#1, j \mid j = 1, 2, 3$ and, consequently, the selection of electricity from the power utility, the diesel generator, and the DC source (i.e., renewable energies and battery) is dynamically performed.

Regarding the fuzzy system theory, the entries x_1 to x_4 are modeled with $V_{x_i} = 2 \mid i = 1, ..., 4$ linguistic terms {LOW, HIGH}, while the entry x_5 is modeled with $V_{x_5} = 3$ linguistic terms {LOW, MEDIUM, HIGH}. Also, each output is modeled with $V_{y_j} = 2 \mid j = 1, 2, 3$ linguistic terms {ON, OFF}. The use of a small number of linguistic terms in the antecedents aims to come up with a low-cost hardware development of the Mamdani T1FS-based controller. Concerning the membership functions of the antecedents, each configuration $\#u$ are associated with different parameters $m_{F_i^l}$ and $\sigma_{F_i^l}$. On the other hand, the parameters $m_{G_j^l}$ and $\sigma_{G_j^l}$ for the membership functions of the consequences are the same for all configurations $\#u$. Concerning the design rules, the Mamdani T1FS is designed with $M = 10$ rules (R^1 to R^{10}), comprising four (4) complete and six (6) incomplete ones. This number of rules cover the mapped possibility to perform the dynamic control of the chosen sources of energy, which agree with the opinion of a specialist.

Note that each rule was created based on the premise that only one energy source will feed a macro BS during a certain period of time. We believe that the best solution may result from the combination of all available sources of energy, however, it will result in a much more complex control technique and more expensive SmartControl devices. Focusing on reducing the complexity of the whole solution, the combination of all available sources of energy is not considered in this thesis. Moreover, based on the premise of being as green as a possible solution for feeding a macro BS, the preferred energy sources to feed a macro BS are solar and wind ones, followed by the power utility and, finally, the diesel generator (the biggest polluter). Also, this order refers to the fact that the cost among them increases in that order.

The designed fuzzy rules are shown in Table 2. Note that in the designed fuzzy rules, the power utility feeds the macro BS and the SmartControl $\#1, 3$ device is triggered if the battery charging level is above 90%, see rules R^3 and R^4. This rule was conceived to extend the battery lifetime and save the stored energy for dealing with potential feeding failures provoked by the power utility. Moreover, the diesel generator will only be used if there is a failure in the feeding provided by the power utility and the battery charging level is low, see rule R^9.

Furthermore, Table 3 lists the parameters for the membership functions of the antecedents and the consequences, when the rules come from a specialist. As a example, Figure 14 shows the membership functions of the antecedents for configuration #4 while Figure 15 shows the membership functions of the consequences for all configurations #u. For the sake of clarity, the values of parameters of the Mamdani T1FS for the detailed configurations are organized in Appendix A.
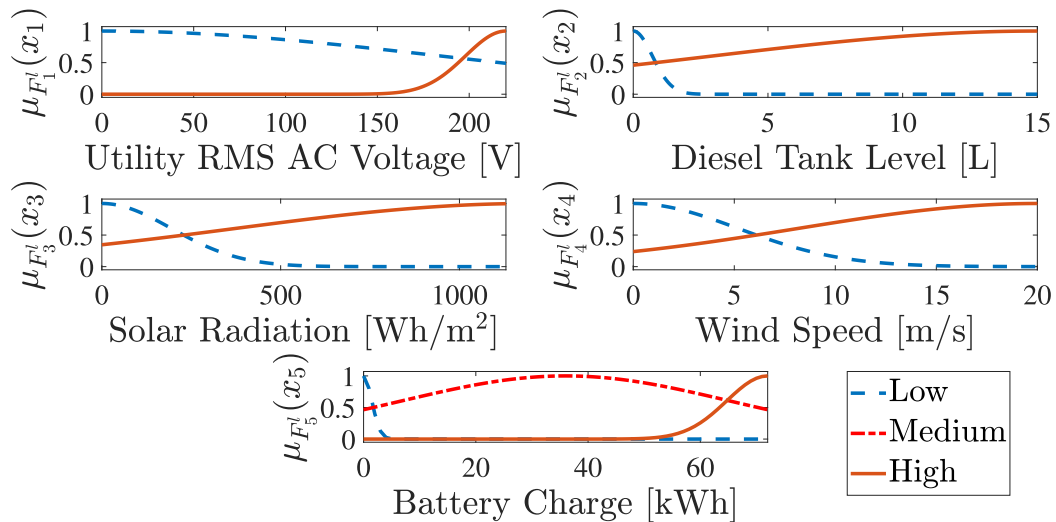
Figure 14 – The membership functions of the antecedents for configuration #4.
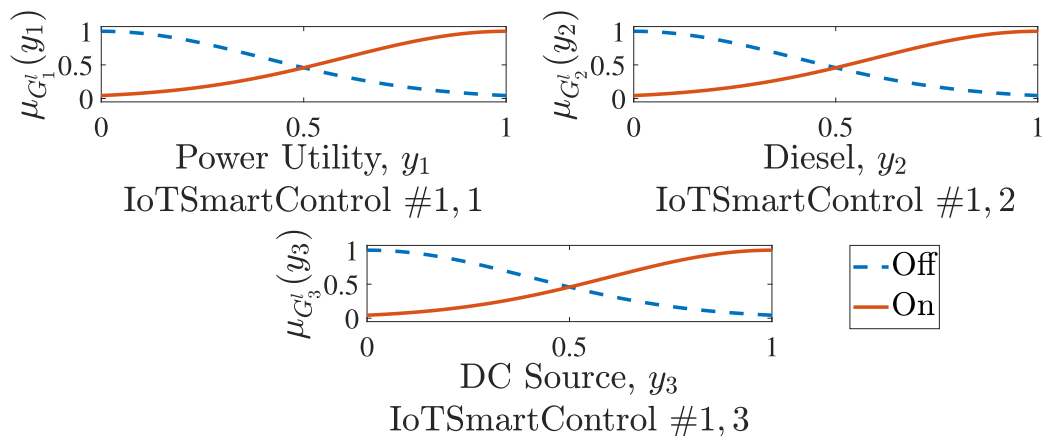
Figure 15 – The membership functions of the consequences for configurations #u | $u = 1, ..., 6$.

Table 2 – The designed fuzzy rules R^1 to R^{10} for the Mamdani T1FS.

	Antecedents					Consequences		
	x_1	x_2	x_3	x_4	x_5	y_1	y_2	y_3
R^1	LOW	-	-	-	MEDIUM	OFF	OFF	ON
R^2	LOW	-	-	-	HIGH	OFF	OFF	ON
R^3	HIGH	-	-	-	MEDIUM	ON	OFF	OFF
R^4	HIGH	-	-	-	HIGH	OFF	OFF	ON
R^5	LOW	LOW	LOW	LOW	LOW	OFF	OFF	OFF
R^6	LOW	LOW	LOW	HIGH	LOW	OFF	OFF	ON
R^7	LOW	LOW	HIGH	LOW	LOW	OFF	OFF	ON
R^8	LOW	LOW	HIGH	HIGH	LOW	OFF	OFF	ON
R^9	LOW	HIGH	-	-	LOW	OFF	ON	OFF
R^{10}	HIGH	-	-	-	LOW	ON	OFF	OFF

Table 3 – The parameters for the membership functions of the antecedents, $m_{F_i^l}$ and $\sigma_{F_i^l}$, and for the membership functions of the consequences, $m_{G_j^l}$ and $\sigma_{G_j^l}$.

	Antecedents					Consequences		
	x_1	x_2	x_3	x_4	x_5	y_1	y_2	y_3
R_1	$m_{F_1^1}, \sigma_{F_1^1}$	-	-	-	$m_{F_5^1}, \sigma_{F_5^1}$	$m_{G_1^1}, \sigma_{G_1^1}$	$m_{G_2^1}, \sigma_{G_2^1}$	$m_{G_3^1}, \sigma_{G_3^1}$
R_2	$m_{F_1^2}, \sigma_{F_1^2}$	-	-	-	$m_{F_5^2}, \sigma_{F_5^2}$	$m_{G_1^2}, \sigma_{G_1^2}$	$m_{G_2^2}, \sigma_{G_2^2}$	$m_{G_3^2}, \sigma_{G_3^2}$
R_3	$m_{F_1^3}, \sigma_{F_1^3}$	-	-	-	$m_{F_5^3}, \sigma_{F_5^3}$	$m_{G_1^3}, \sigma_{G_1^3}$	$m_{G_2^3}, \sigma_{G_2^3}$	$m_{G_3^3}, \sigma_{G_3^3}$
R_4	$m_{F_1^4}, \sigma_{F_1^4}$	-	-	-	$m_{F_5^4}, \sigma_{F_5^4}$	$m_{G_1^4}, \sigma_{G_1^4}$	$m_{G_2^4}, \sigma_{G_2^4}$	$m_{G_3^4}, \sigma_{G_3^4}$
R_5	$m_{F_1^5}, \sigma_{F_1^5}$	$m_{F_2^5}, \sigma_{F_2^5}$	$m_{F_3^5}, \sigma_{F_3^5}$	$m_{F_4^5}, \sigma_{F_4^5}$	$m_{F_5^5}, \sigma_{F_5^5}$	$m_{G_1^5}, \sigma_{G_1^5}$	$m_{G_2^5}, \sigma_{G_2^5}$	$m_{G_3^5}, \sigma_{G_3^5}$
R_6	$m_{F_1^6}, \sigma_{F_1^6}$	$m_{F_2^6}, \sigma_{F_2^6}$	$m_{F_3^6}, \sigma_{F_3^6}$	$m_{F_4^6}, \sigma_{F_4^6}$	$m_{F_5^6}, \sigma_{F_5^6}$	$m_{G_1^6}, \sigma_{G_1^6}$	$m_{G_2^6}, \sigma_{G_2^6}$	$m_{G_3^6}, \sigma_{G_3^6}$
R_7	$m_{F_1^7}, \sigma_{F_1^7}$	$m_{F_2^7}, \sigma_{F_2^7}$	$m_{F_3^7}, \sigma_{F_3^7}$	$m_{F_4^7}, \sigma_{F_4^7}$	$m_{F_5^7}, \sigma_{F_5^7}$	$m_{G_1^7}, \sigma_{G_1^7}$	$m_{G_2^7}, \sigma_{G_2^7}$	$m_{G_3^7}, \sigma_{G_3^7}$
R_8	$m_{F_1^8}, \sigma_{F_1^8}$	$m_{F_2^8}, \sigma_{F_2^8}$	$m_{F_3^8}, \sigma_{F_3^8}$	$m_{F_4^8}, \sigma_{F_4^8}$	$m_{F_5^8}, \sigma_{F_5^8}$	$m_{G_1^8}, \sigma_{G_1^8}$	$m_{G_2^8}, \sigma_{G_2^8}$	$m_{G_3^8}, \sigma_{G_3^8}$
R_9	$m_{F_1^9}, \sigma_{F_1^9}$	$m_{F_2^9}, \sigma_{F_2^9}$	-	-	$m_{F_5^9}, \sigma_{F_5^9}$	$m_{G_1^9}, \sigma_{G_1^9}$	$m_{G_2^9}, \sigma_{G_2^9}$	$m_{G_3^9}, \sigma_{G_3^9}$
R_{10}	$m_{F_1^{10}}, \sigma_{F_1^{10}}$	-	-	-	$m_{F_5^{10}}, \sigma_{F_5^{10}}$	$m_{G_1^{10}}, \sigma_{G_1^{10}}$	$m_{G_2^{10}}, \sigma_{G_2^{10}}$	$m_{G_3^{10}}, \sigma_{G_3^{10}}$

Giving the information about the design of the Mamdani T1FS using the centroid defuzzifier, Subsection 5.2.1 discusses the performance of the controller based on the Mamdani T1FS over time and analyzes the time interval that a macro BS experiences a power outage due to the occurrence of a failure of the power utility. In the sequel, Subsection 5.2.2 analyzes the energy reliability considering different fuel backups in the diesel tank and energy backups in the battery bank. And, it considers the availability of energy sources for the chosen set of scenarios.

5.2.1 Mamdani T1FS-based controller response and the time interval for the first power outage

This subsection exemplifies how the dynamic switching among the energy sources that can be obtained by using DataConcentrator and SmartControl devices. To do so, scenario #1 and the Mamdani T1FS with configuration #6 were chosen. Figure 16 shows the inputs x_i, $i = 1, ..., 5$, the binary outputs y_{d_j}, $j = 1, 2, 3$, and the power outage information related to the macro BS during May of 2019. Note that the performance of the fuzzy system-based controller over time and the time interval for the occurrence of a power outage in the macro BS due to the failure of the power utility are shown. In addition, the time intervals in which the power utility, the diesel generator or the battery bank are supplying the macro BS are shown in Figure 16(b).

According to Figure 16, in the period from May 1st up to 5th, the Mamdani T1FS performs the switching between the power utility and the battery bank. Note that Figure 16(a) shows the battery charge over time and Figure 16(b) shows the control between the power utility and the battery bank, in which logic value 1 means ON and 0 means OFF. This control occurs based on membership functions and rules defined by the specialist. In this regard, if the level of the battery bank is between 90% and 100% of its maximum load, then the Mamdani T1FS chooses the battery bank to feed the macro BS. It occurs because there is a rule to avoid wasting the energy generated by solar and wind sources. On the other hand, there are rules to ensure the availability of energy backup in the case of failure of the power utility.

Regarding an energy reliability analysis, the TTPO value (see details in Section 4.7), which refers to the time interval up to a power outage occurrence in a macro BS is taken into account. In this sense, Figure 16(a) shows the supplying interruption performed by the power utility on May 5th, see the curve associated with the input x_1. The dynamics show that the solar and wind generations were able to feed the macro BS from May 5th through 10th (i.e., 133 hours). From May 10th through 12th, the diesel generator was activated by the Mamdani T1FS to feed the macro BS because the energy stored in the battery bank reached the minimum allowed level. As a consequence, the diesel generator supplied the macro BS for additional 38 hours before the occurrence of the first power
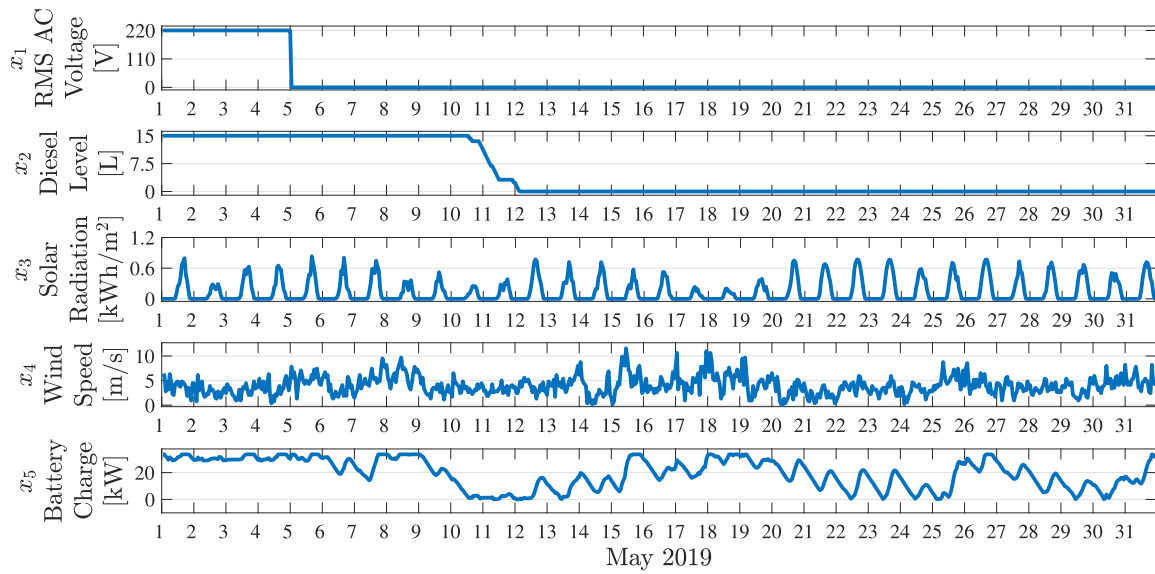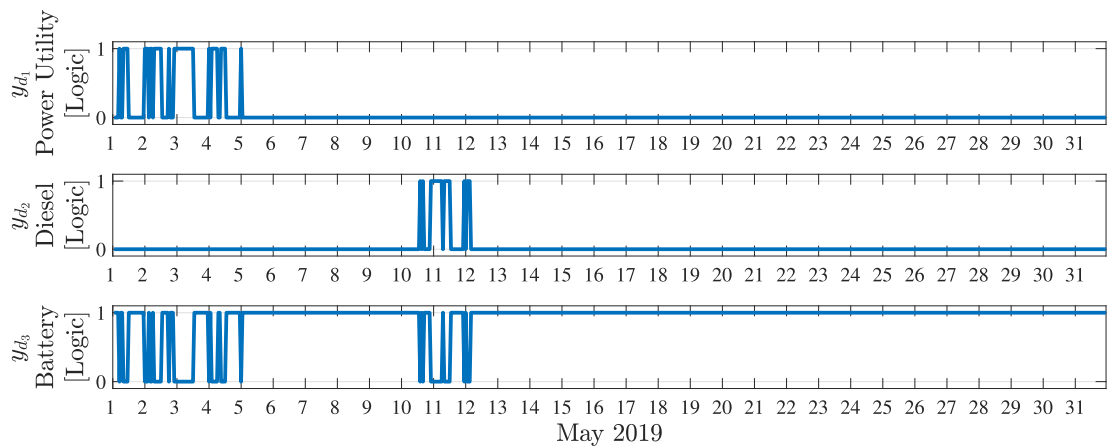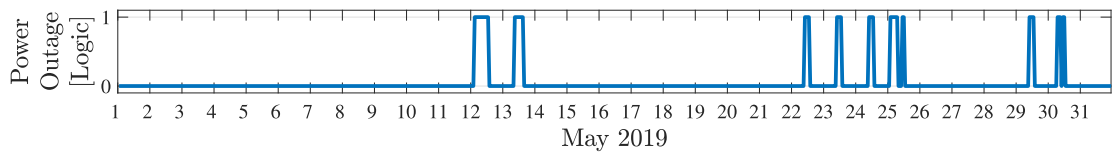
Figure 16 – (a) the inputs of the Mamdani T1FS, (b) the binary outputs of the decision-maker, and (c) the information of power outage in the macro BS.

outage of the macro BS. Precisely, at 4:00 a.m. on May 12th, the shutdown of the macro BS occurred, see Figure 16(c). In this scenario, the TTPO value in the macro BS is equal to $133 + 38 = 171$ hours.

5.2.2   The analysis in term of the reliability function

In this subsection, the energy reliability of a macro BS is assessed using the concepts presented in Subsection 4.7. Also, aiming to provide more examples, all configurations $\#u \mid u = 1, ..., 6$ are considered. In addition, all scenarios $\#v \mid v = 1, ..., 7$ that are typically found in a macro BS are addressed.

To carry out the numerical simulations, the start time of power interruptions provoked by the power utility is modeled as a uniform RV in the time interval delimited by midnight of January 1st and midnight of December 1st, 2019. In the sequel, $N_X = 2680$ samples of this RV are generated for each combination of scenario $\#v$ and the configuration $\#u$. Note that $N_X = 2680$ is a heuristic choice that allows us to carry out the necessary simulations to perform the reliability analysis. Note that it is assumed that the interruption of the power utility supply remains up to the end of this year (i.e., it is a permanent failure).

The numerical simulations result in $N_X = 2680$ sample-values of the RV TTPO for each combination of scenario $\#v$ and the configuration $\#u$ (i.e., $\{X_{uv,m}\}_{m=1}^{2680}$, in which $X_{uv,m}$ is the m-th sample of this RV). According to Section 4.7, the TTPO values can be modeled using the *three*-parameter Weibull PDF [76]. Assuming the number of samples of the TTPO RV is finite and all such samples are equally probable, then the mean (MTTPO), $\mu_{t_{uv}}$, and the standard deviation, $\sigma_{t_{uv}}$, values for configuration $\#u$ and the scenario $\#v$ can be estimated by using

$$\mu_{t_{uv}} = \frac{1}{N_X} \sum_{m=1}^{N_X} X_{uv,m} \tag{5.1}$$

and

$$\sigma_{t_{uv}} = \sqrt{\frac{1}{N_X} \sum_{m=1}^{N_X} (X_{uv,m} - \mu_{t_{uv}})^2} \tag{5.2}$$

which are used to calculate the three parameters of the Weibull PDF. The estimated parameters of the Weibull PDFs that are discussed in the following paragraphs are in Appendix B.

Figure 17 shows the histogram of the RV TTPO and its corresponding fitted *three*-parameters Weibull PDF for scenario $\#1$ combined with the configuration $\#u \mid u = 2, 3, 5, 6$. Note that configurations $\#1$ and $\#4$ are not shown because they do not result in power outages of the macro BS during the year of 2019. In fact, with a 24-hour of energy backup in the battery bank, which represents 1600 Ah (76.8 kWh), the battery bank can store enough energy for feeding the macro BS uninterruptedly the aforementioned configurations. Moreover, Figure 18 shows the curves of the energy reliability for scenario $\#1$ and the configurations $\#u \mid u = 1, ..., 6$. Note that configurations $\#1$ and $\#4$ offer 100% of energy reliability because the Mamdani T1FS can control the switching among

Figure 17 – The histograms of TTPO values and the corresponding fitted *three*-parameters Weibull PDF, $f_1^u(t)$, for scenario #1 and the configurations $\#u \mid u = 2, 3, 5, 6$.

Figure 18 – The reliability function, $R_1^u(t)$, for scenario #1 and the configurations $\#u \mid u = 1, ..., 6$.

the available sources of energy when the power utility fails and the use of $B = 76.8$ kWh of energy backup in the battery bank contributes to the uninterrupted operation of the macro BS. In other words, if the macro BS is fed by solar and wind generations together with $B = 76.8$ kWh of energy backup in the battery bank, then the charging and discharging of the battery bank do not reach the minimum charging level and, as a consequence, no power outage occurs at macro BS. Also, configurations #2 and #5 show the use of an energy backup in the battery bank of $B = 38.4$ kWh and fuel backups of $D = 30$ L and $D = 15$ L, respectively, in the diesel tank. In addition, configurations #3 and #6 show the use of an energy backup in the battery bank of $B = 33.6$ kWh and fuel backups of $D = 30$ L and $D = 15$ L, respectively, in the diesel tank. As expected, configuration #6 yields the worst results because it owns the lowest amount of fuel backup in the diesel tank and the energy backup in the battery bank.

Figure 19 – The histograms of TTPO values and the corresponding fitted *three*-parameters Weibull PDF, $f_2^u(t)$, for scenario #2 and the configurations #u | $u = 1, ..., 6$.

Figure 20 – The reliability function, $R_2^u(t)$, for scenario #2 and the configurations #u | $u = 1, ..., 6$.

Figure 19 illustrates the histogram of the RV TTPO and its corresponding fitted *three*-parameters Weibull PDF for scenario #2 and the configurations #u | $u = 1, ..., 6$. Also, the parameters of the Weibull PDF are listed in Table 12 in Appendix B. Furthermore, Figure 20 shows the curves of the energy reliability for scenario #2 and the configurations #u | $u = 1, ..., 6$. Note that configurations #1 and #4 achieve better energy reliability than the others because the use of $B = 76.8$ kWh of energy backup in the battery bank. Also, configurations #2 and #5 present intermediate results. The different result between configurations #2 and #5 is due to the amount of fuel backup used in the diesel tank: the former uses $D = 30$ L and the latter $D = 15$ L. In addition, configurations #3 and #6 have the worst results comparing to the other configurations. The different result between configurations #3 and #6 is due to the amount of fuel backup used in the diesel tank: the former uses $D = 30$ L and the latter $D = 15$ L. Similar to the scenario #1, configuration

#6 yields the worst results because it owns the minimum amounts of fuel backup for the diesel tank and energy backup in the battery bank.

Figure 21 – The histograms of TTPO values and the corresponding fitted *three*-parameters Weibull PDF, $f_3^u(t)$, for scenario #3 and the configurations #u | $u = 1, ..., 6$.

Figure 22 – The reliability function, $R_3^u(t)$, for scenario #3 and the configurations #u | $u = 1, ..., 6$.

Figure 21 shows the histogram of the RV TTPO and its corresponding fitted *three*-parameters Weibull PDF for scenario #3 and the configurations #u | $u = 1, ..., 6$. Also, the parameters of the Weibull PDF are listed in Table 13 in Appendix B. Furthermore, Figure 22 shows the curves of the energy reliability for scenario #3 and the configurations #u | $u = 1, ..., 6$. Note that the configurations #1 and #4 offer improved energy reliability than the others because they use $B = 76.8$ kWh of energy backup in the battery bank. Similar to the scenarios previously reported, configurations #2 and #5 exhibit intermediate results. Configurations #2 and #5 present a difference due to the amount of fuel backup used in the diesel tank: the former uses $D = 30$ L and the latter $D = 15$ L. Also,

configurations #3 and #6 display the worst results comparing to the other configurations. The different result between configurations #3 and #6 is due to the amount of fuel backup used in the diesel tank: the former uses $D = 30$ L and the latter $D = 15$ L. Again, configuration #6 attains the worst result because it makes use of the minimum amounts of fuel backup in the diesel tank and energy backup in the battery bank.

Figure 23 – The histograms of TTPO values and the corresponding fitted *three*-parameters Weibull PDF, $f_4^u(t)$, for scenario #4 and the configurations $\#u \mid u = 2, 3$.

Figure 24 – The reliability function, $R_4^u(t)$, for scenario #4 and the configurations $\#u \mid u = 1, 2, 3$.

Similar to previous scenarios, Figure 23 portrays the histogram of the RV TTPO and its corresponding fitted *three*-parameters Weibull PDF for scenario #4 and the configurations $\#u \mid u = 2, 3$. Also, the parameters of the Weibull PDF are listed in Table 14 in Appendix B. Note that configuration #1 is not shown because it overcomes power outages in the macro BS during the year of 2019. In fact, with a 24-hour of energy backup in the battery bank, which corresponds to 1600 Ah (76.8 kWh), it can store enough energy for feeding the macro BS uninterruptedly. In addition, scenario #4 using the configurations $\#u \mid u = 1, 2, 3$ present equal results using configurations $\#u \mid u = 4, 5, 6$, respectively. This occurs because scenario #4 does not make use of a diesel generator. In this sense, Figure 24 shows the curves of the energy reliability for scenario #4 and the configurations $\#u \mid u = 1, 2, 3$. Note that the configuration #1 offers 100% of energy reliability because the Mamdani T1FS can control the switching among the available sources of energy when

the power utility fails and the use of $B = 76.8$ kWh of energy backup in the battery bank guarantees the uninterrupted operation of the macro BS. In other words, if the macro BS is fed by a solar and wind generations combined with $B = 76.8$ kWh of energy backup in the battery bank, then the charging and discharging of the battery bank do not reach the minimum charging level and, as a consequence, any power outages occur during the year. Also, configuration #2 makes use of $B = 38.4$ kWh energy backup in the battery bank and, as a consequence, it achieves a better performance in comparison to configuration #3; however, it is far from the performance associated with configuration #1. The lowest performance is offered by configuration #3 because it handles the smallest amount of energy backup in the battery bank.
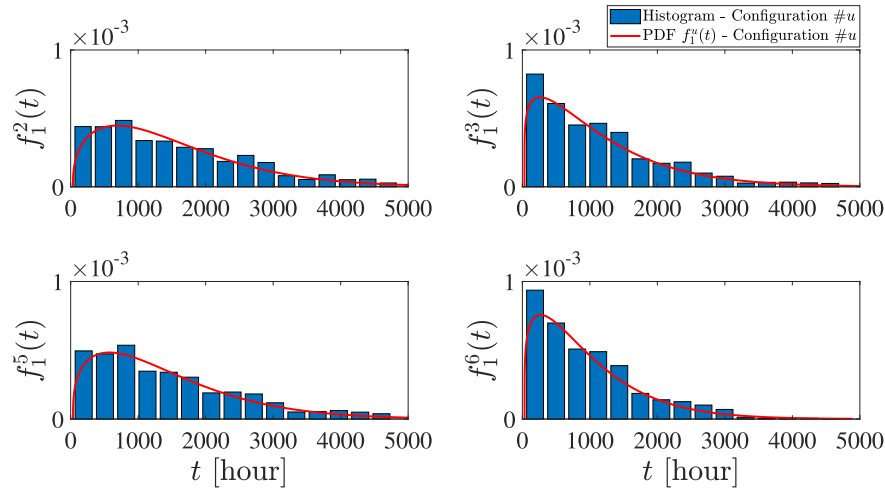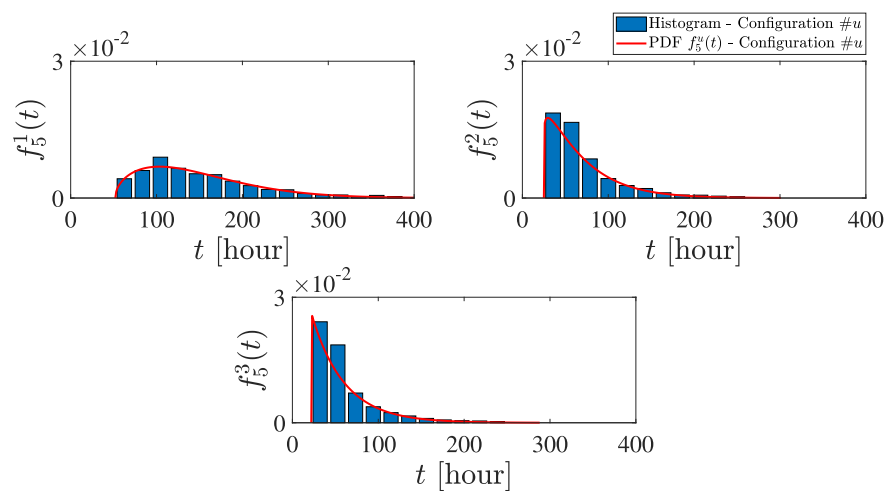

Figure 25 – The histograms of TTPO values and the corresponding fitted *three*-parameters Weibull PDF, $f_5^u(t)$, for scenario #5 and the configurations $\#u \mid u = 1, 2, 3$.
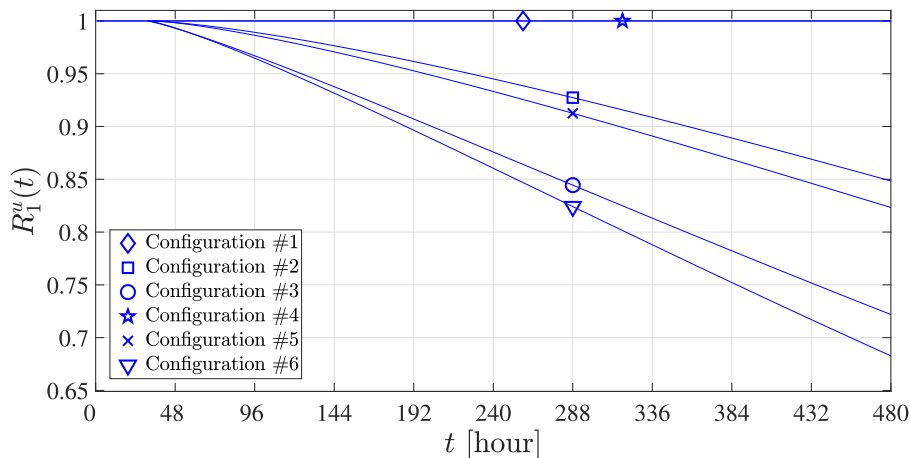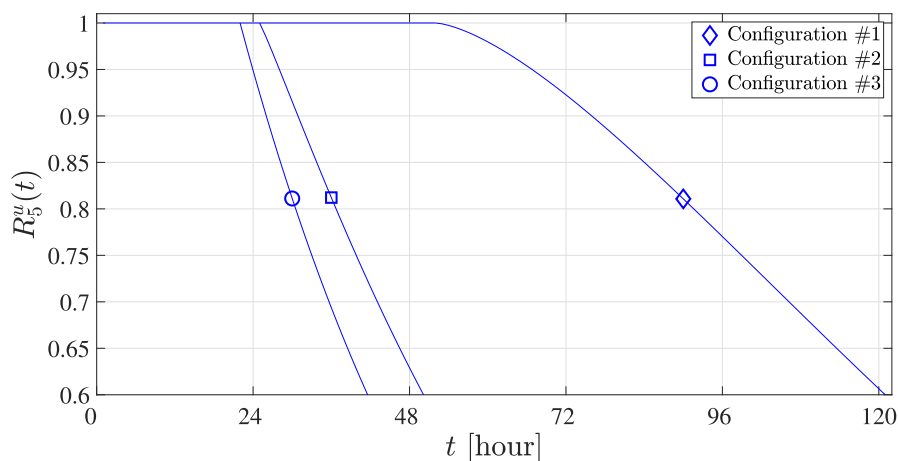

Figure 26 – The reliability function, $R_5^u(t)$, for scenario #5 and the configurations $\#u \mid u = 1, 2, 3$.

Figure 25 illustrates the histogram of the RV TTPO and its corresponding fitted *three*-parameters Weibull PDF for scenario #5 and the configurations $\#u \mid u = 1, 2, 3$.

Also, the parameters of the Weibull PDF are listed in Table 15 in Appendix B. Due to the scenario #5 does not make use of a diesel generator, configurations $\#u \mid u = 1, 2, 3$ present equal results of the configurations $\#u \mid u = 4, 5, 6$, respectively. Furthermore, Figure 26 shows the curves of the energy reliability for scenario #5 and the configurations $\#u \mid u = 1, 2, 3$. Also, configuration #2 shows the use of an energy backup in the battery bank of $B = 38.4$ kWh and it has medium performance when compared to the other configurations. As expected, configuration #3 yield the worst results, because it has the least amount of availability of energy backup in the battery bank.
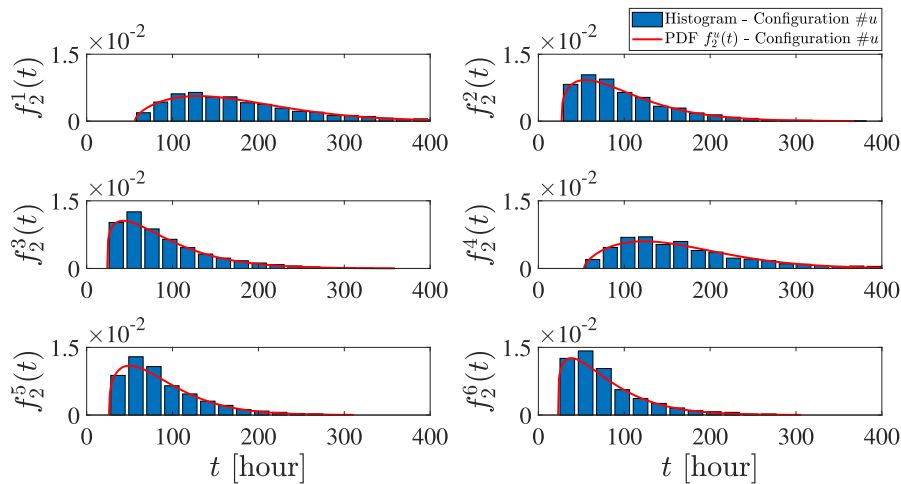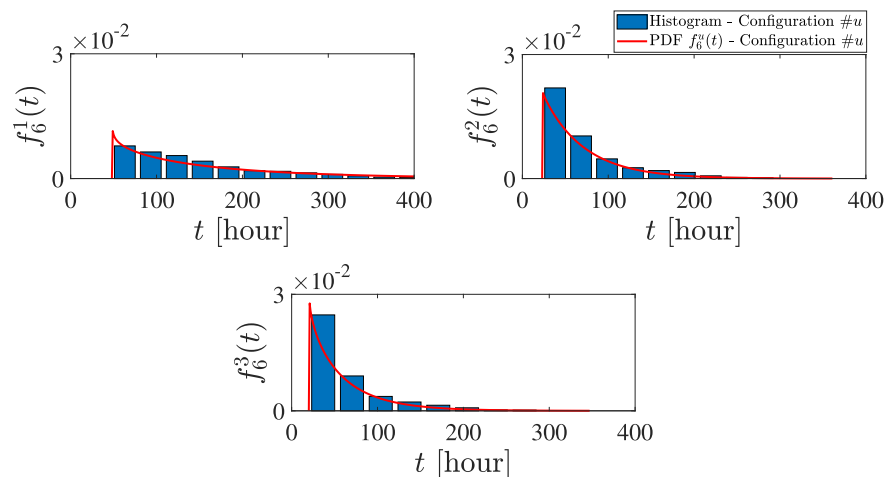

Figure 27 – The histograms of TTPO values and the corresponding fitted *three*-parameters Weibull PDF, $f_6^u(t)$, for scenario #6 and the configurations $\#u \mid u = 1, 2, 3$.
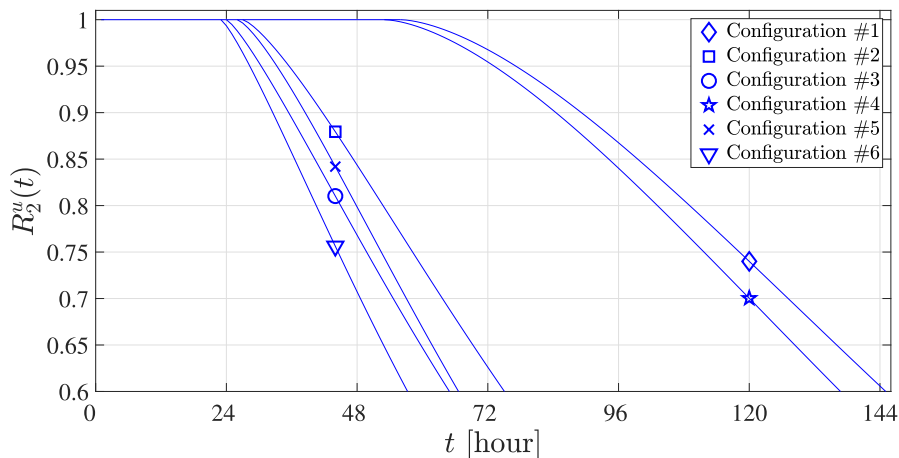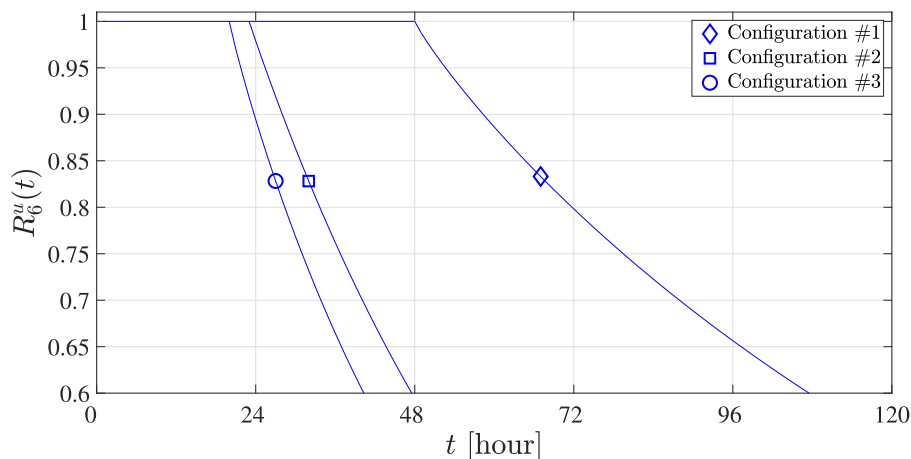

Figure 28 – The reliability function, $R_6^u(t)$, for scenario #6 and the configurations $\#u \mid u = 1, 2, 3$.

Similarly, Figure 27 shows the histogram of the RV TTPO and its corresponding fitted *three*-parameters Weibull PDF for scenario #6 and the configurations $\#u \mid u = 1, 2, 3$. Also, the parameters of the Weibull PDF are listed in Table 16 in Appendix B. Note that

the scenario #6 does not make use of a diesel generator and, consequently, configurations $\#u \mid u = 1, 2, 3$ present equal results of the configurations $\#u \mid u = 4, 5, 6$, respectively. As a result, Figure 28 shows the curves of the energy reliability for scenario #6 and the configurations $\#u \mid u = 1, 2, 3$. Note that the configuration #2 is associated with $B = 38.4$ kWh energy backup in the battery bank and, as a consequence, it performs a little better than configuration #3; however, it far behind the configuration #2. Again, configuration #3 yields attains the lowest performance because it makes use of the minimum amount of energy backup in the battery bank.
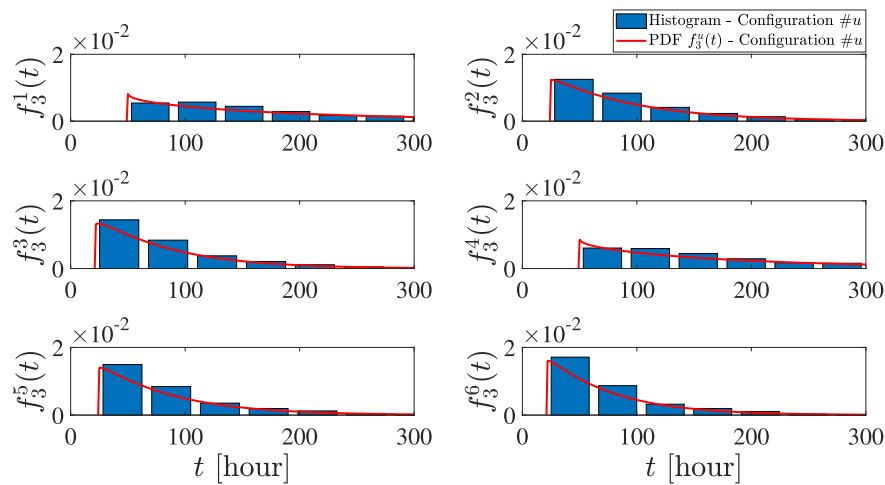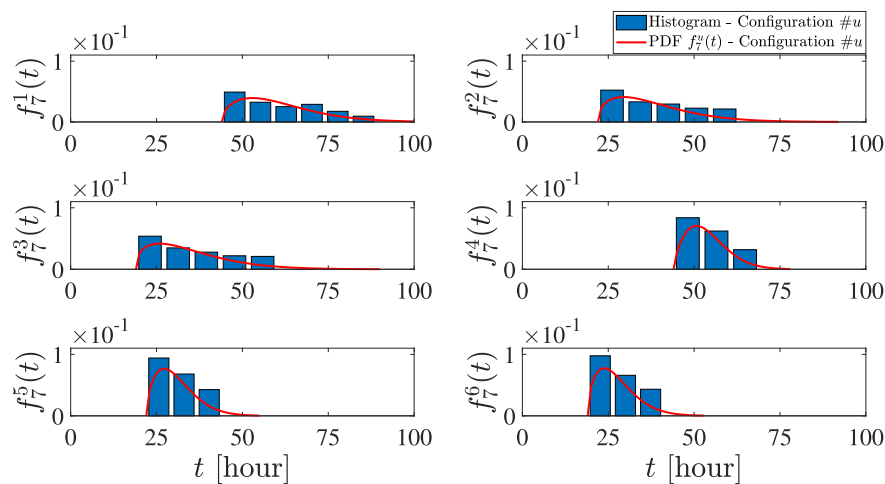

Figure 29 – The histograms of TTPO values and the corresponding fitted *three*-parameters Weibull PDF, $f_7^u(t)$, for scenario #7 and the configurations $\#u \mid u = 1, ..., 6$.
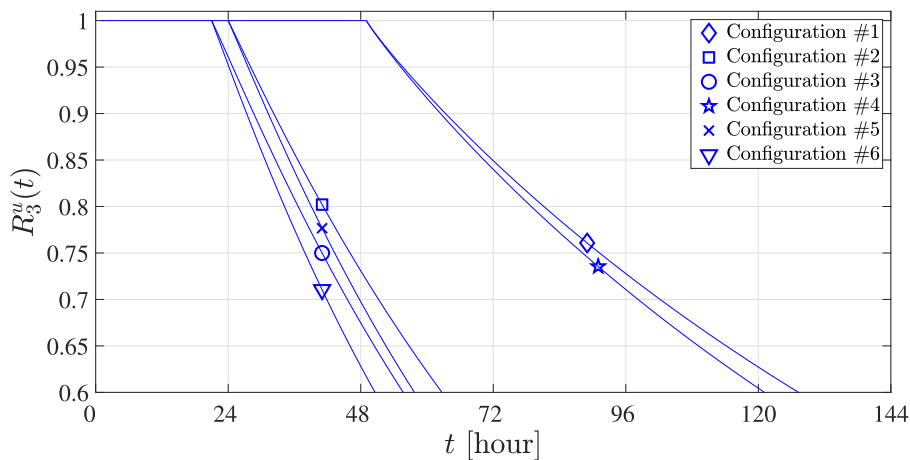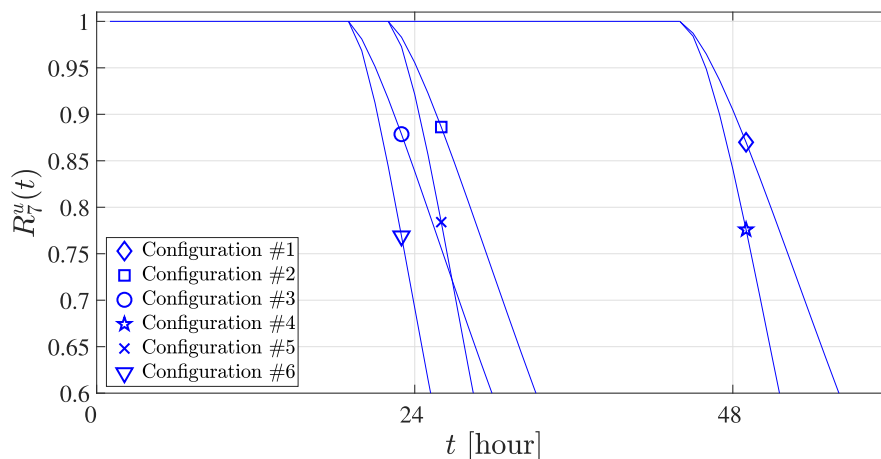

Figure 30 – The reliability function, $R_7^u(t)$, for scenario #7 and the configurations $\#u \mid u = 1, ..., 6$.
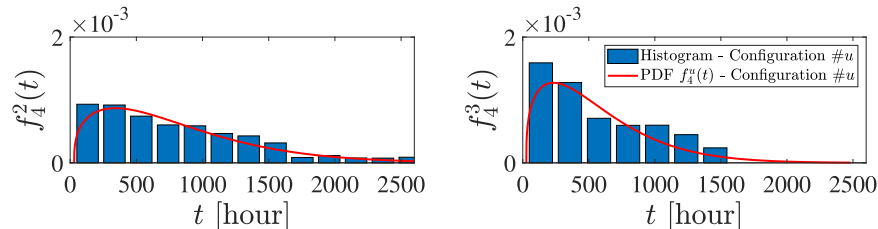
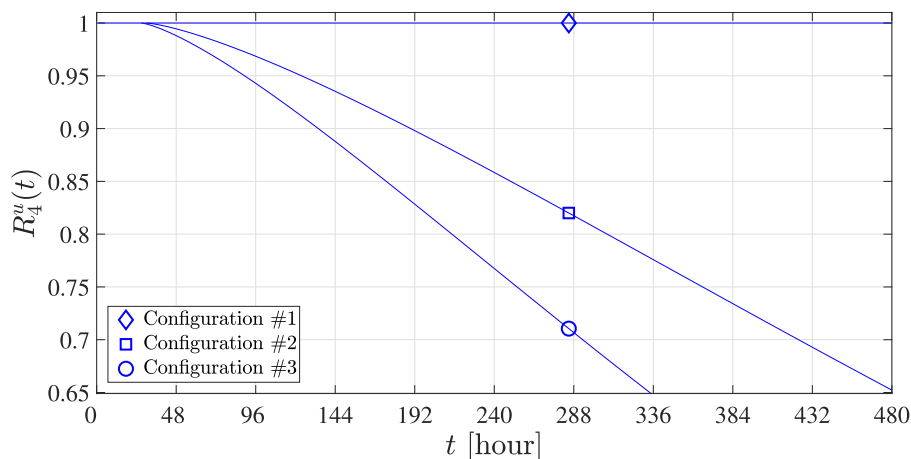Figure 29 shows the histogram of the RV TTPO and its corresponding fitted *three*-parameters Weibull PDF for scenario #7 and the configurations $\#u \mid u = 1, ..., 6$. Also, the parameters of the Weibull PDF are listed in Table 17 in Appendix B. Furthermore,

Figure 30 shows the curves of the energy reliability for scenario #7 and the configurations #u | $u = 1, ..., 6$. Note that the configurations #1 and #4 perform better energy reliability than the others because it makes use of $B = 76.8$ kWh of energy backup in the battery bank. Furthermore, configurations #2 and #5 exhibit intermediate results when compared to the other configurations. Regarding the differences in results between the configurations #2 and #5, this is due to the amount of fuel backup used in the diesel tank: the former uses $D = 30$ L and the latter $D = 15$ L. Also, configurations #3 and #6 display the worst results comparing to the other configurations. Again, regarding the differences in results between the configurations #3 and #6, this is due to the amount of fuel backup used in the diesel tank: the former uses $D = 30$ L and the latter $D = 15$ L. Again, as expected, configuration #6 yield the worst results. This is due to the least amount of availability of fuel backup for the diesel tank and energy backup in the battery bank.

A fair comparison among the discussed scenarios shows that the scenario #7 yields the worst results because only the diesel generator and the battery bank are available for feeding the macro BS when the power utility fails. In addition, the emphasis on solar generation in scenarios #2 and #5 shows a soft decrease in energy reliability functions over time. Moreover, scenarios #3 and #6, which focuses on the wind source of energy, show that the energy reliability functions presents relevant decays over time, mainly when only the wind generation is available, see the curves for scenario #6. Furthermore, scenarios #2 and #5 offer higher energy reliability than scenarios #3 and #6 because the solar generation is less random and offer more energy than the wind one in the city of Juiz de Fora. Also, scenario #2 attains better energy reliability than scenario #5 because the former makes use of a diesel generator. In fact, the use of a diesel generator improves the energy reliability in scenarios #2 and #3 in comparison to scenarios #5 and #6. Additionally, the use of a solar generation together with a diesel generator (i.e., the scenario #2) achieves a considerable gain in terms of energy reliability in comparison to scenario using only the solar generation (i.e., the scenario #5) because the solar energy is generated during the daylight and during the night the diesel generator can be used when the energy of the battery bank runs out. Finally, but not least, the use of the wind generation together with a diesel generator (i.e., the scenario #3) is not comparable to scenario with only a wind generation (i.e., the scenario #6) because the energy produced by the wind generation in the city of Juiz de Fora is low and more random in comparison to the energy produced by the solar generation. In fact, it is necessary to have a minimum value of the wind speed to produce electricity from the wind.

5.3 THE HEIGHT AND CENTROID DEFUZZIFIERS: PERFORMANCE COMPARISON

This section presents the results related to the use of the height defuzzifier to calculate the output of the Mamdani T1FS. Also, it compares the performance of the Mamdani T1FS with the height defuzzifier and its version with the centroid defuzzifier. In this case, the Mamdani T1FS is the one discussed in Section 5.2. The performance comparison among both defuzzifier is discussed because the use of the height defuzzifier demands less computational burden in comparison to the centroid defuzzifier.

Table 4 lists the 96 parameters of the Mamdani T1FS with the height defuzzifier. The initial values of the antecedents parameters $\mu_{F_i^l}(k)$ and $\sigma_{F_i^l}(k)$, and the height defuzzifier parameters $\theta_j^l(k)$ are show in Table 18 in Appendix C. Note that the initial values for the parameters of the antecedents are the same from the Mamdani T1FS with centroid defuzzifier, which is a good strategy starting the training procedure with the steepest descent method.

Regarding the numerical simulation, it focuses on the configuration #6 (see details in Section 5.1), which considers the use of $D = 15$ L of fuel backup in the diesel tank and $B = 33.6$ kWh of energy backup in the battery bank. This is the configuration that presented the worst results in terms of energy reliability how showed in Section 5.2. Note that this configuration was chosen to perform this analysis, but it is worth stating that similar results can be attained considering the other configurations.

Table 4 – The antecedents parameters, $m_{F_i^l}$ and $\sigma_{F_i^l}$, and height parameters, θ_j^l, to be optimized.

	Antecedents					Height		
	x_1	x_2	x_3	x_4	x_5	y_1	y_2	y_3
R_1	$m_{F_1^1}, \sigma_{F_1^1}$	-	-	-	$m_{F_5^1}, \sigma_{F_5^1}$	θ_1^1	θ_2^1	θ_3^1
R_2	$m_{F_1^2}, \sigma_{F_1^2}$	-	-	-	$m_{F_5^2}, \sigma_{F_5^2}$	θ_1^2	θ_2^2	θ_3^2
R_3	$m_{F_1^3}, \sigma_{F_1^3}$	-	-	-	$m_{F_5^3}, \sigma_{F_5^3}$	θ_1^3	θ_2^3	θ_3^3
R_4	$m_{F_1^4}, \sigma_{F_1^4}$	-	-	-	$m_{F_5^4}, \sigma_{F_5^4}$	θ_1^4	θ_2^4	θ_3^4
R_5	$m_{F_1^5}, \sigma_{F_1^5}$	$m_{F_2^5}, \sigma_{F_2^5}$	$m_{F_3^5}, \sigma_{F_3^5}$	$m_{F_4^5}, \sigma_{F_4^5}$	$m_{F_5^5}, \sigma_{F_5^5}$	θ_1^5	θ_2^5	θ_3^5
R_6	$m_{F_1^6}, \sigma_{F_1^6}$	$m_{F_2^6}, \sigma_{F_2^6}$	$m_{F_3^6}, \sigma_{F_3^6}$	$m_{F_4^6}, \sigma_{F_4^6}$	$m_{F_5^6}, \sigma_{F_5^6}$	θ_1^6	θ_2^6	θ_3^6
R_7	$m_{F_1^7}, \sigma_{F_1^7}$	$m_{F_2^7}, \sigma_{F_2^7}$	$m_{F_3^7}, \sigma_{F_3^7}$	$m_{F_4^7}, \sigma_{F_4^7}$	$m_{F_5^7}, \sigma_{F_5^7}$	θ_1^7	θ_2^7	θ_3^7
R_8	$m_{F_1^8}, \sigma_{F_1^8}$	$m_{F_2^8}, \sigma_{F_2^8}$	$m_{F_3^8}, \sigma_{F_3^8}$	$m_{F_4^8}, \sigma_{F_4^8}$	$m_{F_5^8}, \sigma_{F_5^8}$	θ_1^8	θ_2^8	θ_3^8
R_9	$m_{F_1^9}, \sigma_{F_1^9}$	$m_{F_2^9}, \sigma_{F_2^9}$	-	-	$m_{F_5^9}, \sigma_{F_5^9}$	θ_1^9	θ_2^9	θ_3^9
R_{10}	$m_{F_1^{10}}, \sigma_{F_1^{10}}$	-	-	-	$m_{F_5^{10}}, \sigma_{F_5^{10}}$	θ_1^{10}	θ_2^{10}	θ_3^{10}

The training procedure is divided into two parts: data generation and training & validation. The former refers to the use of the Mamdani T1FS with the centroid defuzzifier, which offer good accuracy, to generate $N = N_1 + N_2$ outputs of $y_j^{(k)} \mid j = 1, ..., 3, k = 1, ..., N$. The later performs the training procedure based on E epochs with the data set constituted by the N_1 first input-output pairs. At the end of each epoch, occurs the validation using

the other N_2 input-output pairs. For the performance evaluation during the training & validation procedure, the Mean Square Error (MSE) is applied. The MSE value for the j-th output is giving by

$$MSE_{y_j} = \frac{1}{N_2} \sum_{k=1}^{N_2} \left[y_j(\mathbf{x}^{(k)}) - y_j^{(k)} \right]^2 , \qquad (5.3)$$

where $y_j \left(\mathbf{x}^{(k)} \right)$ is the j-th output of the Mamdani T1FS using the height defuzzifier and $y_j^{(k)}$ is the desired value for the j-th output.

In this regard, for optimizing the parameters for height defuzzifier are generate $N = 4000$ data of input $\mathbf{x}^{(k)} = [x_1^{(k)}, x_2^{(k)}, x_3^{(k)}, x_4^{(k)}, x_5^{(k)}]$ modeled as random variable uniformly distributed according to the universe of $X_1, X_2, X_3, X_4,$ and X_5. Based on this generated input data set, the outputs $y_1^{(k)}$, $y_2^{(k)}$, and $y_3^{(k)}$ are found by using the centroid defuzzifier. In this sense, this data set generated is used as reference of input and output data for the supervised training based on the steepest descent method. For this purpose, the $N = 4000$ input-output pairs are divided into 75% for training ($N_1 = 3000$) and 25% for validation ($N_2 = 1000$). Also, the simulation considers $\beta = 0.1$, and the training is finished after $E = 300$ epochs.

The MSE values of the outputs y_1, y_2, and y_3 after each epoch is shown in Figure 31. Note that MSE_{y_3} attains a fast convergence to the value 0.00007, while MSE_{y_1} and MSE_{y_2} have convergence to the values 0.00015 and 0.00008, respectively. Also, the use of $E = 300$ epochs is because after it the values of MSE_{y_j} stop decreasing. The values of the antecedents parameters ($\mu_{F_i^l}(k)$ and $\sigma_{F_i^l}(k)$), and the height defuzzifier parameters ($\theta_j^l(k)$) obtained with the training procedure after $E = 300$ epochs are listed in Table 19 in Appendix C.

Aiming to compare the results of the use of the parameters updated in the Mamdani T1FS with the height defuzzifier, Figure 32 shows the energy reliability curves of the Mamdani T1FS with the height defuzzifier and the one using centroid defuzzifier presented in Section 5.2 considering the scenarios $\#v \mid v = 1, ..., 7$ for these two defuzzifiers. The curves show an excellent agreement among the performances of the Mamdani T1FS with the height and centroid defuzzifiers. As a consequence, it is clear that the height defuzzifier can substitute the centroid one in the Mamdani T1FS.

Finally, the use of the height defuzzifier is very suitable for the Mamdani T1FS used in this macro BS, once the height defuzzifier compared with the centroid defuzzifier is very similar and the former generates a reduction in computational complexity.

5.4 SUMMARY

This chapter addressed numerical analyses for supporting the carried out discussions in the previous chapters. In this regard, it shown numerical results on the control switching
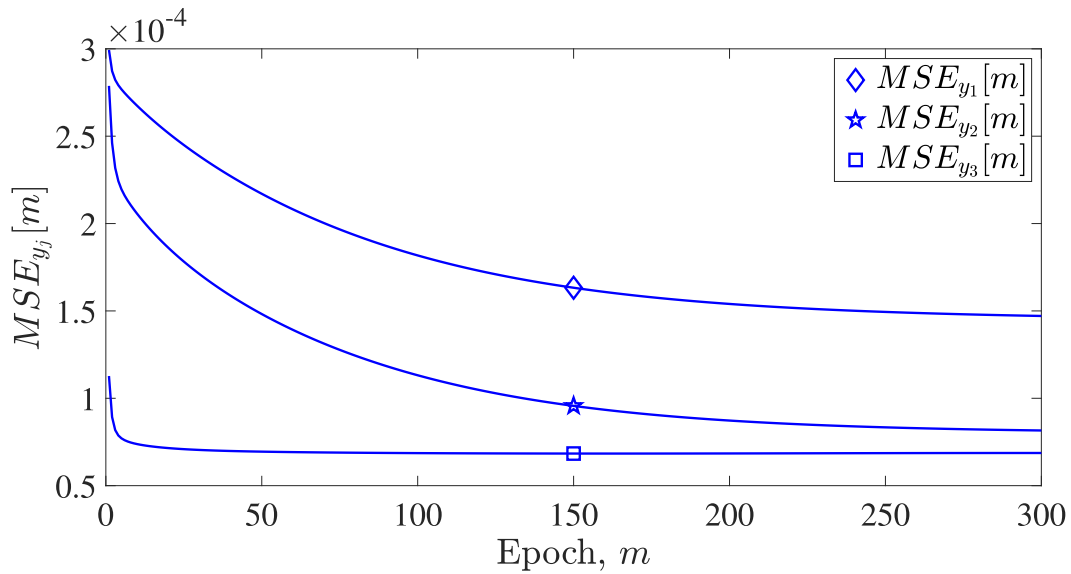
Figure 31 – MSE after each epoch of training.
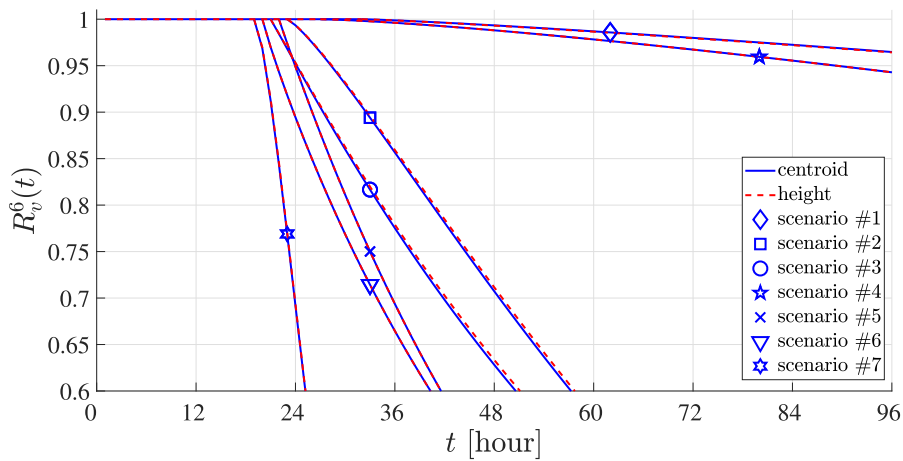
Figure 32 – The reliability function, $R_v^6(t)$, for scenario $\#v \mid v = 1, ..., 7$ and the configuration $\#6$.

among the sources of energy using the Mamdani T1FS. Also, it presented the curves of energy reliability for several configurations and the scenarios typical in a macro BSs. Finally, it compared the results of the Mamdani T1FS using the centroid defuzzifier and the height defuzzifier.

6 CONCLUSIONS

This thesis discussed a feasible solution for improving energy reliability in BSs. Also, it described specific device prototypes and a cloud platform designed for monitoring and managing the available sources of energy. Also, a controller based on the Mamdani T1FS for switching among the sources of energy that are available to feed a macro BS.

In this regard, chapter 2 introduced the investigated problem that is the interruptions in the communications services caused by power outages in BSs. Aiming to deal with this problem, it was detailed a feasible solution for improving energy reliability (i.e., power outages mitigation) in macro BSs, which can be easily adapted to perform the same tasks in other kinds of BS. This feasible solution relied on the use of well-established concepts related to the IoT together with well-known technologies to offer a very simple solution that can be used to retrofit the existing macro BSs and to design new ones. It described that the feasible solution relies on a wireline data network together with actuators inside of BSs for acquiring data related to physical quantities (e.g., environmental temperature, RMS current level, RMS voltage level, wind speed, solar radiation, diesel tank level, and battery charging level). Also, it briefly detailed a cloud SmartPlatform that receives the data set, processes and informs power outages, reports current conditions of the macro BS to the telecommunication companies. Also, the description of prototyped devices to develop the feasible solution was detailed. Overall, it was shown that it is possible to come up with a feasible solution for macro BSs with simple devices and a cloud-based platform to retrofit existing macro BSs or to improve the design of new ones.

Chapter 3 discussed the fuzzy system-based controller in the DataConcentrator device that is responsible for switching the sources of energy in a macro BS. In this regard, it paid attention to the Mamdani T1FS, which was chosen to perform the control task. Based on the choice of the fuzzy theory, the information were gathered by NetSensors devices from the power utility, solar generation, wind generation, diesel generator, and battery bank and were modeled as linguistic terms. This information are temperature, RMS current, RMS voltage, wind speed, solar radiation, diesel tank level, and battery charging level. Also, this chapter discussed the development of two defuzzifiers to obtain the outputs of the fuzzy system. In this sense, the centroid and height defuzzifiers were detailed. The former defuzzifier was chosen because it can be very precise and provide the initialization of the latter for its design. Note that the height defuzzifier is also chosen because it can offer lower computational complexity in comparison to the centroid defuzzifier. In addition, a description of the use of supervised training based on the steepest descent method for updating the parameters of the designed Mamdani T1FS was presented. Overall, this chapter emphasized that the data collected by NetSensors devices can be used by a controller based on the Mamdani T1FS, which is supposed to be developed in the DataConcentrator device, for effectively switching among the available

energy sources in a macro BS. Also, it highlighted that the Mamdani T1FS with the height defuzzifier is, from a computational complexity perspective, a better option for real-time devices in comparison to its counterpart based on the centroid defuzzifier.

Aiming to validate the feasible solution, making use of the Mandani T1FS, for ensuring energy reliability in a macro BS , Chapter 4 presented a power consumption model for a macro BS, which consists of constant and time-varying components, being the latter the one that varies in accord with the data transmission dynamics. Also, this chapter provided the necessary information about the sources of energy considered in this investigation, which are power utility, diesel generator, solar generation, and wind generation. In addition, it briefly discussed about the constraint to assemble a battery bank with battery packs for a macro BS. Information about wind speed and solar radiation in accord with the Brazilian National Institute of Meteorology [64] for the city of Juiz de Fora, Brazil, was provided. Moreover, it proposed the use of the reliability theory for assessing, in a statistical sense, the energy reliability when different sources of energy feed a macro BS and some of them fail. Aiming to achieve a precise energy reliability analysis, it focused on the use of the *three*-parameters Weibull PDF to model the reliability function.

Chapter 5 described numerical analyses that aims to support the carried out discussions in the previous chapters. First, it presented numerical results related to the use of the Mamdani T1FS with the centroid defuzzifier for managing the switching among the sources of energy in a macro BS. In the sequel, it showed the performance of the fuzzy system-based controller over time and analyzed the time interval that macro BS experiences a power outage when a permanent interruption of the power utility takes place. In addition, it analyzed the energy reliability considering different fuel backups in the diesel generator tank and energy backups in the battery bank. To do so, it considered typical scenarios for using distinct combinations of energy sources in a macro BS. It was noted that the Mamdani T1FS using the centroid defuzzifier performs the switching among the energy sources in a macro BS. Also, it detailed numerical results addressing the use of the steepest descent method for obtaining the parameters of the Mamdani T1FS based on the height defuzzifier. After that, it showed a performance comparison between the Mamdani T1FS with the centroid defuzzifier and its counterpart based on the height defuzzifier and concluded that the Mamdani T1FS with the height defuzzifier performs similar to the Mamdani T1FS with the centroid defuzzifier. This performance can be accomplished if the steepest descent method and the initialization of the Mamdani T1FS with the height defuzzifier is based on the parameter values of the Mamdani T1FS with the centroid defuzzifier. Giving such a similar performance, the use of the Mamdani T1FS with the height defuzzifier is highly recommended because it demands less computational burden. The numerical results also showed that the statistical model based on the reliability function is a very powerful tool for evaluating the energy reliability in a macro BS. Also, it can assist telecommunication companies to simulate different scenarios and come up

with solutions to reduces or eliminate the financial and penalty losses related to power outages in BSs because it is possible to perform predictions considering distinct scenarios and configurations (e.g., distinct sets of energy sources).

Overall, this thesis showed that the feasible solution together with the Mamdani T1FS can be appealing to manage distinct sources of energy in macro BSs and, as a consequence, to ensure energy reliability. Also, the use of the Mamdani T1FS proved to be interesting because it can be easily updated and developed in a low-power digital signal processing device. In addition, the numerical results confirmed the relevance of the adoption of the reliability function to analyze the energy reliability in BSs and, as a consequence, to assist telecommunications companies to reduces losses related to power outages in BSs.

6.1 FUTURE WORKS

Future efforts can be toward to:

- implement the Mamdani T1FS in the DataConcentrator device using the same inputs, outputs, Gaussian membership functions, rule base, and height defuzzifier presented in this thesis.

- evaluate the use of other input variables in the Mamdani T1FS such as the electricity price of the power utility, diesel oil price, time of day, RMS AC current, and temperature.

- investigate the behavior of the outputs considering additive noise corruption and loss of some measurement data. In this context, the idea is to apply non-singleton T1FS, and singleton and non-singleton T2FS.

REFERENCES

[1] L. D. Xu, W. He, and S. Li, "Internet of things in industries: A survey," *IEEE Transaction on Industrial Informatics*, vol. 10, no. 4, pp. 2233–2243, Nov. 2014.

[2] L. de M. B. A. Dib, G. R. Colen, M. de L. Filomeno, and M. V. Ribeiro, "Orthogonal chirp division multiplexing for baseband data communication systems," *IEEE Systems Journal*, vol. 14, no. 2, pp. 2164–2174, Jul. 2020.

[3] R. M. de Oliveira, A. B. Vieira, H. A. Latchman, and M. V. Ribeiro, "Medium access control protocols for power line communication: A survey," *IEEE Communications Surveys Tutorials*, vol. 21, no. 1, pp. 920–939, Aug. 2019.

[4] S. P. Mohanty, U. Choppali, and E. Kougianos, "Everything you wanted to know about smart cities: The internet of things is the backbone," *IEEE Consumer Electronics Magazine*, vol. 5, no. 3, pp. 60–70, Aug. 2016.

[5] Y. Saleem, N. Crespi, M. H. Rehmani, and R. Copeland, "Internet of things-aided smart grid: Technologies, architectures, applications, prototypes, and future research directions," *IEEE Access*, vol. 7, pp. 62 962–63 003, Apr. 2019.

[6] V. L. R. da Costa, V. Fernandes, and M. V. Ribeiro, "Narrowband hybrid PLC/wireless: Transceiver prototype, hardware resource usage and energy consumption," *Ad Hoc Networks*, vol. 94, p. 101945, Nov. 2019.

[7] T. R. Oliveira, C. A. G. Marques, M. S. Pereira, S. L. Netto, and M. V. Ribeiro, "The characterization of hybrid PLC-wireless channels: A preliminary analysis," in *2013 IEEE 17th International Symposium on Power Line Communications and Its Applications*, Jun. 2013, pp. 98–102.

[8] L. d. M. B. A. Dib, V. Fernandes, M. de L. Filomeno, and M. V. Ribeiro, "Hybrid PLC/wireless communication for smart grids and internet of things applications," *IEEE Internet of Things Journal*, vol. 5, no. 2, pp. 655–667, Oct. 2018.

[9] V. Fernandes, H. V. Poor, and M. V. Ribeiro, "A hybrid power line/wireless dual-hop system with energy harvesting relay," *IEEE Internet of Things Journal*, vol. 5, no. 5, pp. 4201–4211, Jul. 2018.

[10] A. H. Mohd Aman, E. Yadegaridehkordi, Z. S. Attarbashi, R. Hassan, and Y. Park, "A survey on trend and classification of internet of things reviews," *IEEE Access*, vol. 8, pp. 111 763–111 782, Jun. 2020.

[11] M. Nicola, Z. Alsafi, C. Sohrabi, A. Kerwan, A. Al-Jabir, C. Iosifidis, M. Agha, and R. Agha, "The socio-economic implications of the coronavirus pandemic (covid-19): A review," *International Journal of Surgery*, vol. 78, pp. 185 – 193, Jun. 2020.

[12] O. S. Matompo, "Legal protection of online business transaction (e-commerce) during the covid-19 pandemic in indonesia," *Legal Standing: Jurnal Ilmu Hukum*, vol. 4, no. 1, pp. 146–154, May 2020.

[13] B. Shen, Z. Lei, X. Huang, and Q. Chen, "An interference contribution rate based small cells on/off switching algorithm for 5G dense heterogeneous networks," *IEEE Access*, vol. 6, pp. 29 757–29 769, May 2018.

[14] ANATEL, "Plano estrutural de redes de telecomunicações," Internet: https://www. anatel.gov.br/dados/pert, [Sep. 12, 2020].

[15] J. Kartite and M. Cherkaoui, "Study of the different structures of hybrid systems in renewable energies: A review," *Energy Procedia*, vol. 157, pp. 323 – 330, Jan. 2019.

[16] G. Auer, O. Blume, V. Giannini, I. Godor, M. Imran, Y. Jading, E. Katranaras, M. Olsson, D. Sabella, P. Skillermark *et al.*, "Energy efficiency analysis of the reference systems, areas of improvements and target breakdown," *Earth*, vol. 20, no. 10, Dec. 2010.

[17] X. Ge, J. Yang, H. Gharavi, and Y. Sun, "Energy efficiency challenges of 5G small cell networks," *IEEE Communications Magazine*, vol. 55, no. 5, pp. 184–191, May 2017.

[18] M. Deruyck, W. Joseph, and L. Martens, "Power consumption model for macrocell and microcell base stations," *Transactions on Emerging Telecommunications Technologies*, vol. 25, Mar. 2014.

[19] J. Lorincz and T. Matijevic, "On interdependence among transmit and consumed power of macro base station technologies," *Computer Communications*, vol. 50, Sep. 2014.

[20] T. Han and N. Ansari, "Powering mobile networks with green energy," *IEEE Wireless Communications*, vol. 21, no. 1, pp. 90–96, Feb. 2014.

[21] Y.-K. Chia, S. Sun, and R. Zhang, "Energy cooperation in cellular networks with renewable powered base stations," *IEEE Transactions on Wireless Communications*, vol. 13, no. 12, pp. 6996–7010, Dec. 2014.

[22] D. Li, W. Saad, I. Guvenc, A. Mehbodniya, and F. Adachi, "Decentralized energy allocation for wireless networks with renewable energy powered base stations," *IEEE Transactions on Communications*, vol. 63, no. 6, pp. 2126–2142, Jun. 2015.

[23] A. M. Aris and B. Shabani, "Sustainable power supply solutions for off-grid base stations," *Energies*, vol. 8, no. 10, pp. 10 904–10 941, Sep. 2015.

[24] H. A. H. Hassan, A. Pelov, and L. Nuaymi, "Integrating cellular networks, smart grid, and renewable energy: Analysis, architecture, and challenges," *IEEE Access*, vol. 3, pp. 2755–2770, Dec. 2015.

[25] M. S. Hossain, A. Jahid, K. Z. Islam, and M. F. Rahman, "Solar pv and biomass resources-based sustainable energy supply for off-grid cellular base stations," *IEEE Access*, vol. 8, pp. 53 817–53 840, Mar. 2020.

[26] M. Deruyck, D. Renga, M. Meo, L. Martens, and W. Joseph, "Accounting for the varying supply of solar energy when designing wireless access networks," *IEEE Transactions on Green Communications and Networking*, vol. 2, no. 1, pp. 275–290, Mar. 2017.

[27] F. Ahmed, M. Naeem, W. Ejaz, M. Iqbal, and A. Anpalagan, "Resource management in cellular base stations powered by renewable energy sources," *Journal of Network and Computer Applications*, vol. 112, pp. 1–17, Jun. 2018.

[28] Y. Zhang, M. Meo, R. Gerboni, and M. A. Marsan, "Minimum cost solar power systems for LTE macro base stations," *Computer Networks*, vol. 112, pp. 12–23, Jan. 2017.

[29] G. Piro, M. Miozzo, G. Forte, N. Baldo, L. A. Grieco, G. Boggia, and P. Dini, "Hetnets powered by renewable energy sources: Sustainable next-generation cellular networks," *IEEE Internet Computing*, vol. 17, no. 1, pp. 32–39, Jan. 2013.

[30] D. Niyato, X. Lu, and P. Wang, "Adaptive power management for wireless base stations in a smart grid environment," *IEEE Wireless Communications*, vol. 19, no. 6, pp. 44–51, Dec. 2012.

[31] M. H. Alsharif, R. Nordin, and M. Ismail, "Green wireless network optimisation strategies within smart grid environments for long term evolution (lte) cellular networks in malaysia," *Renewable Energy*, vol. 85, pp. 157–170, Jan. 2016.

[32] S.-Y. Lee, C.-Y. Liu, M.-K. Chang, D.-N. Yang, and Y.-W. P. Hong, "Cooperative multicasting in renewable energy enhanced relay networks—expending more power to save energy," *IEEE Transactions on Wireless Communications*, vol. 15, no. 1, pp. 753–768, Sep. 2015.

[33] L. A. Fletscher, L. A. Suárez, D. Grace, C. V. Peroni, and J. M. Maestre, "Energy-aware resource management in heterogeneous cellular networks with hybrid energy sources," *IEEE Transactions on Network and Service Management*, vol. 16, no. 1, pp. 279–293, Aug. 2018.

[34] G. Zhang, Y. Cao, L. Wang, and D. Li, "Operation cost minimization for base stations with heterogenous energy supplies and sleep-awake mode: A two-timescale approach," *IEEE Transactions on Cognitive Communications and Networking*, vol. 4, no. 4, pp. 908–918, Sep. 2018.

[35] H. Wang, Z. Zhao, X. Cheng, J. Ying, J. Qu, and G. Xu, "Base station sleeping strategy for on-grid energy saving in cellular networks with hybrid energy supplies in iot environment," *IEEE Access*, vol. 6, pp. 45 578–45 589, Aug. 2018.

[36] B. Wang, Q. Yang, L. T. Yang, and C. Zhu, "On minimizing energy consumption cost in green heterogeneous wireless networks," *Computer Networks*, vol. 129, pp. 522–535, Dec. 2017.

[37] A. Jahid, M. S. Islam, M. S. Hossain, M. E. Hossain, M. K. H. Monju, and M. F. Hossain, "Toward energy efficiency aware renewable energy management in green cellular networks with joint coordination," *IEEE Access*, vol. 7, pp. 75 782–75 797, Jun. 2019.

[38] V. O. C. Guimaraes, "Incidents in networks that impact on the provision of telecommunications services," Internet: http://slideplayer.com.br/slide/11349872/, [May 01, 2020].

[39] D. Peraković, M. Periša, P. Zorić, and I. Cvitić, "Development and implementation possibilities of 5G in industry 4.0," in *Design, Simulation, Manufacturing: The Innovation Exchange.* Springer, Cham, 2020.

[40] M. L. Robin, "Fire protection in telecommunication facilities," *Process Safety Progress*, vol. 19, no. 2, pp. 107–111, Apr. 2004.

[41] S. Yeh, S. Talwar, G. Wu, N. Himayat, and K. Johnsson, "Capacity and coverage enhancement in heterogeneous networks," *IEEE Wireless Communications*, vol. 18, no. 3, pp. 32–38, Jun. 2011.

[42] ANATEL, "Consulta pública nº 29," Internet: https://sistemas.anatel.gov.br/SACP/Contribuicoes/TextoConsulta.asp?CodProcesso=C2036&Tipo=1&Opcao=andamento, [Sep. 27, 2020].

[43] ANATEL, "Resolução nº 574, de 28 de outubro de 2011," Internet: https://www.anatel.gov.br/legislacao/resolucoes/2011/57-resolucao-574, [Sep. 27, 2020].

[44] ANATEL, "Resolução nº 575, de 28 de outubro de 2011," Internet: https://www.anatel.gov.br/legislacao/resolucoes/2011/68-resolucao-575, [Sep. 27, 2020].

[45] ANATEL, "Resolução nº 717, de 23 de dezembro de 2019," Internet: https://www.anatel.gov.br/legislacao/resolucoes/2019/1371-resolucao-717, [Sep. 27, 2020].

[46] R. Fielding, J. Gettys, J. Mogul, H. Frystyk, L. Masinter, P. Leach, and T. Berners-Lee, "Hypertext transfer protocol–http/1.1," *Internet RFC 2616*, Jun. 1999.

[47] J. M. Mendel, *Uncertain Rule-Based Fuzzy Systems: Introduction and New Directions.*, 2nd ed.   Los Angeles, USA: Springer International Publishing, 2017.

[48] M. Schulz, P. Klapper, M. Hollick, E. Tews, and S. Katzenbeisser, "Trust the wire, they always told me! on practical non-destructive wire-tap attacks against ethernet," in *Association for Computing Machinery*, Jul. 2016, p. 43–48.

[49] Modbus, "The modbus organization," Internet: http://modbus.org/, [May 01, 2020].

[50] T. S. Ustun and S. M. S. Hussain, "Iec 62351-4 security implementations for iec 61850 mms messages," *IEEE Access*, vol. 8, pp. 123 979–123 985, Jun. 2020.

[51] R. Amoah, S. Camtepe, and E. Foo, "Securing dnp3 broadcast communications in scada systems," *IEEE Transactions on Industrial Informatics*, vol. 12, no. 4, pp. 1474–1485, Jul. 2016.

[52] J. . Thomesse, "Fieldbus technology in industrial automation," *Proceedings of the IEEE*, vol. 93, no. 6, pp. 1073–1101, May 2005.

[53] Kyung Chang Lee, Suk Lee, and Man Hyung Lee, "Remote fuzzy logic control of networked control system via profibus-dp," *IEEE Transactions on Industrial Electronics*, vol. 50, no. 4, pp. 784–792, Jul. 2003.

[54] S. Biegacki and D. VanGompel, "The application of devicenet in process control," *ISA Transactions*, vol. 35, no. 2, pp. 169 – 176, Jan. 1996.

[55] S. Davies, "Industrial ethernet - the fundamentals of ethernet/ip - ethernet/ip has reached the million-node landmark, but what is making this protocol so attractive to industrial control engineers?" *Computing Control Engineering Journal*, vol. 18, no. 1, pp. 42–45, Mar. 2007.

[56] R. Pigan and M. Metter, *Automating with PROFINET: Industrial communication based on Industrial Ethernet.*   New Jersey, EUA: John Wiley & Sons, 2008.

[57] M. Knezic, B. Dokic, and Z. Ivanovic, "Topology aspects in ethercat networks," in *Proceedings of 14th International Power Electronics and Motion Control Conference*, Sep. 2010, pp. T1–1–T1–6.

[58] Qilian Liang and J. M. Mendel, "Interval type-2 fuzzy logic systems: theory and design," *IEEE Transactions on Fuzzy Systems*, vol. 8, no. 5, pp. 535–550, Oct. 2000.

[59] E. P. de Aguiar, R. P. Amaral, M. M. Vellasco, and M. V. Ribeiro, "An enhanced singleton type-2 fuzzy logic system for fault classification in a railroad switch machine," *Electric Power Systems Research*, vol. 158, pp. 195 – 206, May 2018.

[60] R. P. F. Amaral, I. F. Menezes, and M. V. Ribeiro, "An extension of the type-1 and singleton fuzzy logic system trained by scaled conjugate gradient methods for multiclass classification problems," *Neurocomputing*, vol. 411, pp. 149 – 163, Oct. 2020.

[61] I. H. Altaş, *Fuzzy Logic Control in Energy Systems with Design Applications in MATLAB/Simulink*. 1st ed. London, United Kingdom: The Institution of Engineering and Technology, 2017.

[62] M. V. Ribeiro, "Learning rate updating methods applied to adaptive fuzzy equalizers for broadband power line communications," *EURASIP J. Appl. Signal Process.*, vol. 2004, no. 16, pp. 2592–2599, Nov. 2004.

[63] E. P. de Aguiar, F. M. de A. Nogueira, M. M. B. R. Vellasco, and M. V. Ribeiro, "Set-membership type-1 fuzzy logic system applied to fault classification in a switch machine," *IEEE Transactions on Intelligent Transportation Systems*, vol. 18, no. 10, pp. 2703–2712, Feb. 2017.

[64] INMET, "Instituto Nacional de Metereologia," Internet: http://www.inmet.gov.br/, [May 01, 2020].

[65] Consul, "Consul ccf07dbbna air condiotioner," Internet: https://loja.consul.com.br/condicionador-de-ar-janela-consul-multi-air-7500-frio-ccf07eb/p, [May 01, 2020].

[66] W. L. Theo, J. S. Lim, W. S. Ho, H. Hashim, and C. T. Lee, "Review of distributed generation (DG) system planning and optimisation techniques: Comparison of numerical and mathematical modelling methods," *Renewable and Sustainable Energy Reviews*, vol. 67, pp. 531–573, Jan. 2017.

[67] N. Solar, "Photovoltaic solar panel 280w - yingli yl280p-29b," Internet: https://www.neosolar.com.br, [May 01, 2020].

[68] V. Nelson, E. Gilmore, and K. Starcher, *Introduction to Wind Energy*. Netherlands: Alternative Energy Institute, 1993.

[69] CEMIG, "Atlas eólico de Minas Gerais," Internet: http://www.cemig.com.br/pt-br/A_Cemig_e_o_Futuro/inovacao/Alternativas_Energeticas/Documents/atlas%20eolico%20MG.pdf, [Sep. 01, 2020].

[70] D. Weisser, "A wind energy analysis of grenada: an estimation using the 'weibull' density function," *Renewable Energy*, vol. 28, no. 11, pp. 1803 – 1812, Sep. 2003.

[71] P. Araujo and M. Marinho, "Analysis of hydro - wind complementarity in state of Pernambuco, Brazil by means of Weibull parameters," *IEEE Latin America Transactions*, vol. 17, no. 04, pp. 556–563, Apr. 2019.

[72] B. W. Co, "Bergey bwc excel 10," Internet: https://en.wind-turbine-models.com/turbines/501-bergey-bwc-excel-10, [Mar. 21, 2020].

[73] R. C. Souza, "Previsão da distribuição da densidade de probabilidade da geração de energia eólica usando técnicas não paramétricas," Ph.D. dissertation, Pontifícia Universidade Católica do Rio de Janeiro, Brazil, 2015.

[74] Toyama, "Diesel generator td7000cx3ed," Internet: http://www.toyama.com.br/, [May 01, 2020].

[75] Changhong, "Ch48100 lifepo, battery pack 48v/100ah," Internet: http://www.changhongbatteries.com/, [May 01, 2020].

[76] M. Rausand and A. Høyland, *System Reliability Theory: Models, Statistical Methods, and Applications*, 2nd ed. Nova York: John Wiley & Sons, 2003.

APPENDIX A – The values of the parameters for the Mamdani T1FS based on the centroid defuzzifier

Table 5 – The values of the parameters for the Mamdani T1FS designed to deal with the configuration #1.

| | Antecedents | | | | | | | | | | Consequences | | | | | |
| | x_1 | | x_2 | | x_3 | | x_4 | | x_5 | | y_1 | | y_2 | | y_3 | |
	$m_{F_1^l}$	$\sigma_{F_1^l}$	$m_{F_2^l}$	$\sigma_{F_2^l}$	$m_{F_3^l}$	$\sigma_{F_3^l}$	$m_{F_4^l}$	$\sigma_{F_4^l}$	$m_{F_5^l}$	$\sigma_{F_5^l}$	$m_{G_1^l}$	$\sigma_{G_1^l}$	$m_{G_2^l}$	$\sigma_{G_2^l}$	$m_{G_3^l}$	$\sigma_{G_3^l}$
R_1	0	184	-	-	-	-	-	-	35348	28682	0	0.4	0	0.4	0.5	0.4
R_2	0	184	-	-	-	-	-	-	76800	6523	0	0.4	0	0.4	0.5	0.4
R_3	220	22	-	-	-	-	-	-	35348	28682	0.5	0.4	0	0.4	0	0.4
R_4	220	22	-	-	-	-	-	-	76800	6523	0	0.4	0	0.4	0.5	0.4
R_5	0	184	0	0.64	0	213	0	5.18	0	1339	0	0.4	0	0.4	0	0.4
R_6	0	184	0	0.64	0	213	20	11.81	0	1339	0	0.4	0	0.4	0.5	0.4
R_7	0	184	0	0.64	1200	806	0	5.18	0	1339	0	0.4	0	0.4	0.5	0.4
R_8	0	184	0	0.64	1200	806	20	11.81	0	1339	0	0.4	0	0.4	0.5	0.4
R_9	0	184	30	24.84	-	-	-	-	0	1339	0	0.4	0.5	0.4	0	0.4
R_{10}	220	22	-	-	-	-	-	-	0	1339	0.5	0.4	0	0.4	0	0.4

Table 6 – The values of the parameters for the Mamdani T1FS designed to deal with the configuration #2.

| | Antecedents | | | | | | | | | | Consequences | | | | | |
| | x_1 | | x_2 | | x_3 | | x_4 | | x_5 | | y_1 | | y_2 | | y_3 | |
	$m_{F_1^l}$	$\sigma_{F_1^l}$	$m_{F_2^l}$	$\sigma_{F_2^l}$	$m_{F_3^l}$	$\sigma_{F_3^l}$	$m_{F_4^l}$	$\sigma_{F_4^l}$	$m_{F_5^l}$	$\sigma_{F_5^l}$	$m_{G_1^l}$	$\sigma_{G_1^l}$	$m_{G_2^l}$	$\sigma_{G_2^l}$	$m_{G_3^l}$	$\sigma_{G_3^l}$
R_1	0	184	-	-	-	-	-	-	38400	3262	0	0.4	0	0.4	0.5	0.4
R_2	0	184	-	-	-	-	-	-	18068	14009	0	0.4	0	0.4	0.5	0.4
R_3	220	22	-	-	-	-	-	-	38400	3262	0.5	0.4	0	0.4	0	0.4
R_4	220	22	-	-	-	-	-	-	18068	14009	0	0.4	0	0.4	0.5	0.4
R_5	0	184	0	0.64	0	213	0	5.18	0	1339	0	0.4	0	0.4	0	0.4
R_6	0	184	0	0.64	0	213	20	11.81	0	1339	0	0.4	0	0.4	0.5	0.4
R_7	0	184	0	0.64	1200	806	0	5.18	0	1339	0	0.4	0	0.4	0.5	0.4
R_8	0	184	0	0.64	1200	806	20	11.81	0	1339	0	0.4	0	0.4	0.5	0.4
R_9	0	184	30	24.84	-	-	-	-	0	1339	0	0.4	0.5	0.4	0	0.4
R_{10}	220	22	-	-	-	-	-	-	0	1339	0.5	0.4	0	0.4	0	0.4

Table 7 – The values of the parameters for the Mamdani T1FS designed to deal with the configuration #3.

	Antecedents										Consequences					
	x_1		x_2		x_3		x_4		x_5		y_1		y_2		y_3	
	$m_{F_1^l}$	$\sigma_{F_1^l}$	$m_{F_2^l}$	$\sigma_{F_2^l}$	$m_{F_3^l}$	$\sigma_{F_3^l}$	$m_{F_4^l}$	$\sigma_{F_4^l}$	$m_{F_5^l}$	$\sigma_{F_5^l}$	$m_{G_1^l}$	$\sigma_{G_1^l}$	$m_{G_2^l}$	$\sigma_{G_2^l}$	$m_{G_3^l}$	$\sigma_{G_3^l}$
R_1	0	184	-	-	-	-	-	-	33600	2854	0	0.4	0	0.4	0.5	0.4
R_2	0	184	-	-	-	-	-	-	15908	12173	0	0.4	0	0.4	0.5	0.4
R_3	220	22	-	-	-	-	-	-	33600	2854	0.5	0.4	0	0.4	0	0.4
R_4	220	22	-	-	-	-	-	-	15908	12173	0	0.4	0	0.4	0.5	0.4
R_5	0	184	0	0.64	0	213	0	5.18	0	1339	0	0.4	0	0.4	0	0.4
R_6	0	184	0	0.64	0	213	20	11.81	0	1339	0	0.4	0	0.4	0.5	0.4
R_7	0	184	0	0.64	1200	806	0	5.18	0	1339	0	0.4	0	0.4	0.5	0.4
R_8	0	184	0	0.64	1200	806	20	11.81	0	1339	0	0.4	0	0.4	0.5	0.4
R_9	0	184	30	24.84	-	-	-	-	0	1339	0	0.4	0.5	0.4	0	0.4
R_{10}	220	22	-	-	-	-	-	-	0	1339	0.5	0.4	0	0.4	0	0.4

Table 8 – The values of the parameters for the Mamdani T1FS designed to deal with the configuration #4.

	Antecedents										Consequences					
	x_1		x_2		x_3		x_4		x_5		y_1		y_2		y_3	
	$m_{F_1^l}$	$\sigma_{F_1^l}$	$m_{F_2^l}$	$\sigma_{F_2^l}$	$m_{F_3^l}$	$\sigma_{F_3^l}$	$m_{F_4^l}$	$\sigma_{F_4^l}$	$m_{F_5^l}$	$\sigma_{F_5^l}$	$m_{G_1^l}$	$\sigma_{G_1^l}$	$m_{G_2^l}$	$\sigma_{G_2^l}$	$m_{G_3^l}$	$\sigma_{G_3^l}$
R_1	0	184	-	-	-	-	-	-	35348	28682	0	0.4	0	0.4	0.5	0.4
R_2	0	184	-	-	-	-	-	-	76800	6523	0	0.4	0	0.4	0.5	0.4
R_3	220	22	-	-	-	-	-	-	35348	28682	0.5	0.4	0	0.4	0	0.4
R_4	220	22	-	-	-	-	-	-	76800	6523	0	0.4	0	0.4	0.5	0.4
R_5	0	184	0	0.64	0	213	0	5.18	0	1339	0	0.4	0	0.4	0	0.4
R_6	0	184	0	0.64	0	213	20	11.81	0	1339	0	0.4	0	0.4	0.5	0.4
R_7	0	184	0	0.64	1200	806	0	5.18	0	1339	0	0.4	0	0.4	0.5	0.4
R_8	0	184	0	0.64	1200	806	20	11.81	0	1339	0	0.4	0	0.4	0.5	0.4
R_9	0	184	15	11.5	-	-	-	-	0	1339	0	0.4	0.5	0.4	0	0.4
R_{10}	220	22	-	-	-	-	-	-	0	1339	0.5	0.4	0	0.4	0	0.4

Table 9 – The values of the parameters for the Mamdani T1FS designed to deal with the configuration #5.

| | Antecedents | | | | | | | | | | Consequences | | | | | |
| | x_1 | | x_2 | | x_3 | | x_4 | | x_5 | | y_1 | | y_2 | | y_3 | |
	$m_{F_1^l}$	$\sigma_{F_1^l}$	$m_{F_2^l}$	$\sigma_{F_2^l}$	$m_{F_3^l}$	$\sigma_{F_3^l}$	$m_{F_4^l}$	$\sigma_{F_4^l}$	$m_{F_5^l}$	$\sigma_{F_5^l}$	$m_{G_1^l}$	$\sigma_{G_1^l}$	$m_{G_2^l}$	$\sigma_{G_2^l}$	$m_{G_3^l}$	$\sigma_{G_3^l}$
R_1	0	184	-	-	-	-	-	-	38400	3262	0	0.4	0	0.4	0.5	0.4
R_2	0	184	-	-	-	-	-	-	18068	14009	0	0.4	0	0.4	0.5	0.4
R_3	220	22	-	-	-	-	-	-	38400	3262	0.5	0.4	0	0.4	0	0.4
R_4	220	22	-	-	-	-	-	-	18068	14009	0	0.4	0	0.4	0.5	0.4
R_5	0	184	0	0.64	0	213	0	5.18	0	1339	0	0.4	0	0.4	0	0.4
R_6	0	184	0	0.64	0	213	20	11.81	0	1339	0	0.4	0	0.4	0.5	0.4
R_7	0	184	0	0.64	1200	806	0	5.18	0	1339	0	0.4	0	0.4	0.5	0.4
R_8	0	184	0	0.64	1200	806	20	11.81	0	1339	0	0.4	0	0.4	0.5	0.4
R_9	0	184	15	11.5	-	-	-	-	0	1339	0	0.4	0.5	0.4	0	0.4
R_{10}	220	22	-	-	-	-	-	-	0	1339	0.5	0.4	0	0.4	0	0.4

Table 10 – The values of the parameters for the Mamdani T1FS designed to deal with the configuration #6.

| | Antecedents | | | | | | | | | | Consequences | | | | | |
| | x_1 | | x_2 | | x_3 | | x_4 | | x_5 | | y_1 | | y_2 | | y_3 | |
	$m_{F_1^l}$	$\sigma_{F_1^l}$	$m_{F_2^l}$	$\sigma_{F_2^l}$	$m_{F_3^l}$	$\sigma_{F_3^l}$	$m_{F_4^l}$	$\sigma_{F_4^l}$	$m_{F_5^l}$	$\sigma_{F_5^l}$	$m_{G_1^l}$	$\sigma_{G_1^l}$	$m_{G_2^l}$	$\sigma_{G_2^l}$	$m_{G_3^l}$	$\sigma_{G_3^l}$
R_1	0	184	-	-	-	-	-	-	33600	2854	0	0.4	0	0.4	0.5	0.4
R_2	0	184	-	-	-	-	-	-	15908	12173	0	0.4	0	0.4	0.5	0.4
R_3	220	22	-	-	-	-	-	-	33600	2854	0.5	0.4	0	0.4	0	0.4
R_4	220	22	-	-	-	-	-	-	15908	12173	0	0.4	0	0.4	0.5	0.4
R_5	0	184	0	0.64	0	213	0	5.18	0	1339	0	0.4	0	0.4	0	0.4
R_6	0	184	0	0.64	0	213	20	11.81	0	1339	0	0.4	0	0.4	0.5	0.4
R_7	0	184	0	0.64	1200	806	0	5.18	0	1339	0	0.4	0	0.4	0.5	0.4
R_8	0	184	0	0.64	1200	806	20	11.81	0	1339	0	0.4	0	0.4	0.5	0.4
R_9	0	184	15	11.5	-	-	-	-	0	1339	0	0.4	0.5	0.4	0	0.4
R_{10}	220	22	-	-	-	-	-	-	0	1339	0.5	0.4	0	0.4	0	0.4

APPENDIX B – The parameter of the energy reliability functions.

Table 11 – The values of μ_t, σ_t, ξ, λ and k parameters refer to the scenario#1 and the configurations $\#u \mid u = 2, 3, 5, 6$.

	μ_t	σ_t	ξ	λ	k
Configuration #2	1532.10	1108.80	33.00	1642.40	1.39
Configuration #3	1132.50	948.61	31.00	1164.80	1.18
Configuration #5	1429.90	1069.60	35.00	1518.00	1.33
Configuration #6	960.65	776.49	32.00	990.25	1.21

Table 12 – The values of μ_t, σ_t, ξ, λ and k parameters refer to the scenario#2 and configurations $\#u \mid u = 1, ..., 6$.

	μ_t	σ_t	ξ	λ	k
Configuration #1	177.55	78.90	56.00	135.57	1.60
Configuration #2	100.27	56.40	27.00	79.67	1.33
Configuration #3	89.79	54.07	24.00	70.47	1.24
Configuration #4	166.74	73.18	53.00	126.96	1.61
Configuration #5	87.68	47.21	26.00	67.14	1.34
Configuration #6	78.25	45.60	23.00	59.12	1.23

Table 13 – The values of μ_t, σ_t, ξ, λ and k parameters refer to the scenario#3 and configurations $\#u \mid u = 1, ..., 6$.

	μ_t	σ_t	ξ	λ	k
Configuration #1	215.56	177.95	49.00	161.12	0.93
Configuration #2	98.13	72.75	24.00	74.75	1.02
Configuration #3	86.04	62.63	21.00	66.12	1.04
Configuration #4	200.58	160.46	49.00	147.36	0.94
Configuration #5	88.15	62.59	24.00	64.85	1.03
Configuration #6	77.43	55.17	21.00	57.00	1.02

Table 14 – The values of μ_t, σ_t, ξ, λ and k parameters refer to the scenario#4 and configurations $\#u \mid u = 1, 2$.

	μ_t	σ_t	ξ	λ	k
Configuration #1	804.51	587.34	30.00	844.67	1.35
Configuration #2	557.13	406.52	27.00	576.88	1.33

Table 15 – The values of μ_t, σ_t, ξ, λ and k parameters refer to the scenario#5 and the configurations $\#u \mid u = 1, 2, 3$.

	μ_t	σ_t	ξ	λ	k
Configuration #1	149.71	67.56	52.00	108.17	1.49
Configuration #2	70.21	41.89	25.00	46.66	1.09
Configuration #3	60.41	38.50	22.00	38.37	1.00

Table 16 – The values of μ_t, σ_t, ξ, λ and k parameters refer to the scenario#6 and the configurations $\#u \mid u = 1, 2, 3$.

	μ_t	σ_t	ξ	λ	k
Configuration #1	179.79	145.01	48.00	125.36	0.90
Configuration #2	71.43	48.74	23.00	48.29	0.99
Configuration #3	62.89	45.56	20.00	41.61	0.94

Table 17 – The values of μ_t, σ_t, ξ, λ and k parameters refer to the scenario#7 and the configurations $\#u \mid u = 1, ..., 6$.

	μ_t	σ_t	ξ	λ	k
Configuration #1	61.07	11.88	44.00	18.89	1.48
Configuration #2	38.35	11.93	22.00	17.96	1.41
Configuration #3	35.09	11.97	19.00	17.62	1.38
Configuration #4	53.92	6.03	44.00	11.12	1.72
Configuration #5	30.84	5.83	22.00	9.84	1.57
Configuration #6	27.69	5.91	19.00	9.64	1.52

APPENDIX C – Training based on the the steepest descent method

The initial and final values of the parameters of the Mamdani T1FS based on the height defuzzifier are shown in Tables 18 and 19, respectively.

Table 18 – The initial values of the antecedents' parameters, $m_{F_i^l}$ and $\sigma_{F_i^l}$, and the height parameters, θ_j^l.

| | Antecedents | | | | | | | | | | Height | | |
| | x_1 | | x_2 | | x_3 | | x_4 | | x_5 | | y_1 | y_2 | y_3 |
	$m_{F_1^l}$	$\sigma_{F_1^l}$	$m_{F_2^l}$	$\sigma_{F_2^l}$	$m_{F_3^l}$	$\sigma_{F_3^l}$	$m_{F_4^l}$	$\sigma_{F_4^l}$	$m_{F_5^l}$	$\sigma_{F_5^l}$	θ_1^l	θ_2^l	θ_3^l
R_1	0	184	-	-	-	-	-	-	15908	12173	0.5	0.5	0.5
R_2	0	184	-	-	-	-	-	-	33600	2854	0.5	0.5	0.5
R_3	220	22	-	-	-	-	-	-	15908	12173	0.5	0.5	0.5
R_4	220	22	-	-	-	-	-	-	33600	2854	0.5	0.5	0.5
R_5	0	184	0	0.64	0	213	0	5.18	0	1339	0.5	0.5	0.5
R_6	0	184	0	0.64	0	213	20	11.81	0	1339	0.5	0.5	0.5
R_7	0	184	0	0.64	1200	806	0	5.18	0	1339	0.5	0.5	0.5
R_8	0	184	0	0.64	1200	806	20	11.81	0	1339	0.5	0.5	0.5
R_9	0	184	15	11.5	-	-	-	-	0	1339	0.5	0.5	0.5
R_{10}	220	22	-	-	-	-	-	-	0	1339	0.5	0.5	0.5

Table 19 – The final values of the antecedents parameters, $m_{F_i^l}$ and $\sigma_{F_i^l}$, and the height parameters, θ_j^l, after 300 epochs .

	Antecedents										Height		
	x_1		x_2		x_3		x_4		x_5		y_1	y_2	y_3
	$m_{F_1^l}$	$\sigma_{F_1^l}$	$m_{F_2^l}$	$\sigma_{F_2^l}$	$m_{F_3^l}$	$\sigma_{F_3^l}$	$m_{F_4^l}$	$\sigma_{F_4^l}$	$m_{F_5^l}$	$\sigma_{F_5^l}$	θ_1^l	θ_2^l	θ_3^l
R_1	0.07	184.05	-	-	-	-	-	-	15908.00	12173.00	0.70	0.30	0.30
R_2	0.00	184.00	-	-	-	-	-	-	33600.00	2854.00	0.69	0.31	0.31
R_3	221.15	19.33	-	-	-	-	-	-	15908.00	12173.00	0.69	0.74	0.31
R_4	220.07	21.91	-	-	-	-	-	-	33600.00	2854.00	0.59	0.42	0.31
R_5	0.00	184.00	-0.05	0.59	0.00	213.00	-0.01	5.17	0.00	1339.00	0.69	0.35	0.27
R_6	0.00	184.00	-0.06	0.56	0.00	213.00	20.01	11.81	0.00	1339.00	0.65	0.31	0.31
R_7	0.00	184.00	-0.16	0.48	1200.00	806.00	-0.02	5.16	0.00	1339.00	0.51	0.38	0.29
R_8	0.00	184.00	-0.17	0.41	1200.00	806.00	20.01	11.80	0.00	1339.00	0.55	0.30	0.61
R_9	-0.02	183.99	15.55	11.56	-	-	-	-	-0.02	1338.96	0.29	0.30	0.72
R_{10}	220.12	21.76	-	-	-	-	-	-	0.00	1339.00	0.43	0.72	0.41

APPENDIX D – List of Publications

The list of journal and conference papers published or submitted during the graduate period is as follows:

- C. R. Miranda, F. P. de Campos, and M. V. Ribeiro, "Energy reliability in macro base stations: A feasible solution based on a type-1 Mamdani fuzzy system" Electric Power Systems Research, 2020. (2nd review round)

- C. R. Miranda, F. P. de Campos, and M. V. Ribeiro, "The prototype implementation of an IoT-based framework for energy reliability and asset security in base stations," in *XXXVII Simpósio Brasileiro de Telecomunicações e Processamento de Sinais*, Petrópolis, Oct. 2019.